

# Spatiotemporal Clustering with Neyman-Scott Processes via Connections to Bayesian Nonparametric Mixture Models

Yixin Wang<sup>1,\*</sup>, Anthony Degleris<sup>2,\*</sup>, Alex H. Williams<sup>3,4</sup>, and Scott W. Linderman<sup>5,†</sup>

January 17, 2022

## Abstract

Neyman-Scott processes (NSPs) are point process models that generate clusters of points in time or space. They are natural models for a wide range of phenomena, ranging from neural spike trains to document streams. The clustering property is achieved via a doubly stochastic formulation: first, a set of latent events is drawn from a Poisson process; then, each latent event generates a set of observed data points according to another Poisson process. This construction is similar to Bayesian nonparametric mixture models like the Dirichlet process mixture model (DPMM) in that the number of latent events (i.e. clusters) is a random variable, but the point process formulation makes the NSP especially well suited to modeling spatiotemporal data. While many specialized algorithms have been developed for DPMMs, comparatively fewer works have focused on inference in NSPs. Here, we present novel connections between NSPs and DPMMs, with the key link being a third class of Bayesian mixture models called mixture of finite mixture models (MFMMs). Leveraging this connection, we adapt the standard collapsed Gibbs sampling algorithm for DPMMs to enable scalable Bayesian inference on NSP models. We demonstrate the potential of Neyman-Scott processes on a variety of applications including sequence detection in neural spike trains and event detection in document streams.

## 1 Introduction

Many natural systems give rise to discrete sets of events in time and space. Slipping tectonic plates produce a sequence of shocks along the plate boundary. Galaxies appear as clustered speckles of light in astronomical surveys. Social networks produce time-stamped messages with text and images. In all of these examples, observed events tend to cluster together: earthquake aftershocks are spatially and temporally localized, galaxies are pulled together by gravity, and world events give rise to groups of related messages.

---

<sup>1</sup> Department of Statistics, University of Michigan, Ann Arbor, MI, USA

<sup>2</sup> Department of Electrical Engineering, Stanford University, Stanford, CA, USA

<sup>3</sup> Center for Neural Science, New York University, New York, NY, USA

<sup>4</sup> Center for Computational Neuroscience, Flatiron Institute, New York, NY, USA

<sup>5</sup> Department of Statistics and Wu Tsai Neurosciences Institute, Stanford University, Stanford, CA, USA

\* Equal Contribution

† Corresponding Author: [scott.linderman@stanford.edu](mailto:scott.linderman@stanford.edu)

Neyman-Scott processes (NSPs) [Neyman and Scott, 1958] are point processes that capture this clustering property. First, a set of *latent events* is drawn from a Poisson process. Then, each latent event adds an *impulse response* to the intensity function of another Poisson process, which produces the set of *observed events*. For example, a latent event might represent the location of a galaxy and its size, shape, age, etc., and the impulse response determines the distribution over the location, size, and type of the stars in that galaxy, which are the observed events. If the impulse responses are localized in time and space, then each latent event produces a cluster of observed events.

Inferring the location and properties of underlying latent events is often of scientific interest. However, this can be challenging from a statistical perspective, since neither the number of latent events nor their locations are known. Traditionally, inference and estimation in NSPs has been approached with reversible jump Markov chain Monte Carlo (RJMCMC) algorithms, which use birth and death moves [Green, 2003] to address this trans-dimensional inference problem [Møller and Waagepetersen, 2003]. However, in practice, RJMCMC can suffer from high rejection rates, sacrificing performance unless proposals are carefully crafted. Alternatively, there a number of specialized algorithms based on minimum contrast estimation, which optimize the parameters of the NSP to match statistics of the data, such as Ripley’s K-function [Ripley, 1977] or the pair correlation function [Bartlett, 1963, Cressie, 1993, Stoyan and Stoyan, 1996, Møller and Waagepetersen, 2003, Waagepetersen, 2007, Diggle, 2013, Baddeley et al., 2015]. Though these estimators may be asymptotically consistent, they may produce biased estimates with finite sample sizes, and their theoretical properties are still an area of study. Further, obtaining closed-form expressions for these second-order statistics often requires strong assumptions about the parametric form of the NSP. For example, several methods assume that clusters are spatially isotropic and of equal size in expectation [Tanaka et al., 2008], and subsequent research has aimed to relax these constraints [Tanaka and Ogata, 2014, Møller and Toftaker, 2014].

Here, we establish a novel connection between NSPs and Bayesian nonparametric mixture models, and in doing so we inherit the host of Bayesian inference algorithms that have been developed for the latter [Neal, 2000, Jain and Neal, 2004, Blei and Jordan, 2006, Jain and Neal, 2007, Miller and Harrison, 2018]. Intuitively, latent events are akin to clusters in a mixture model. The key observation is that in an NSP, the number of latent events is a Poisson random variable thanks to the Poisson process construction. In this regard, the NSP differs from the Dirichlet process mixture model (DPMM) — the canonical Bayesian nonparametric mixture model — since a DPMM produces a countably infinite number of clusters. Instead, the NSP more closely resembles the mixture of finite mixture model (MFMM), which assumes an explicit prior distribution on the number of clusters [Nobile, 1994, Phillips and Smith, 1996, Richardson and Green, 1997, Miller and Harrison, 2018]. In an NSP, that prior is a Poisson distribution and, in contrast to other MFMMs, its mean is tuned to the volume of space or time under consideration, making the NSP especially well-suited to spatiotemporal modeling.

In this paper, we will formalize the connection between Neyman-Scott processes and mixture of finite mixture models. Furthermore, we show how Dirichlet process mixture models arise as a limiting form of an NSP, and in doing so we bridge MFMMs and DPMMs. We exploit the novel connection to derive a collapsed Gibbs sampling algorithm like that of Neal [2000] and Miller and Harrison [2018], which operates directly on partitions of data points. Finally, we demonstrate the efficacy of this algorithm on simulated data and in applications to sequence detection in multineuronal spike train recordings and event detection in document streams.

## 2 Neyman-Scott Processes

Point processes are probabilistic models that yield random finite sets of points  $\{x_n\}_{n=1}^N \subset \mathcal{X}$ , where  $\mathcal{X}$  is a compact subset of  $\mathbb{R}^D$ , e.g. of space or time [Daley and Vere-Jones, 2003]. The simplest point process is the Poisson process [Kingman, 1992], which is governed by a nonnegative intensity function  $\lambda(x) : \mathcal{X} \mapsto \mathbb{R}_+$ . The number of events that fall in a region  $\mathcal{X}' \subseteq \mathcal{X}$  follows a Poisson distribution with mean  $\int_{\mathcal{X}'} \lambda(x) dx$ . Moreover, the number of events in  $\mathcal{X}'$  is independent of the number in  $\mathcal{X}''$  if  $\mathcal{X}'$  and  $\mathcal{X}''$  are disjoint. We use the notation  $\{x_n\}_{n=1}^N \sim \text{PP}(\lambda(x))$  to indicate that a set  $\{x_n\}_{n=1}^N$  is drawn from a Poisson process with intensity function  $\lambda(x)$ .

A *marked* point process is a multidimensional point process that generates sets of tuples  $\{(x_n, y_n)\}_{n=1}^N \subset \mathcal{X} \times \mathcal{Y}$ . A marked Poisson process is simply a Poisson process on this extended space with an intensity function  $\lambda(x, y)$ . Just like the sum and product rules for joint densities, we can factor the intensity into a product  $\lambda(x, y) = \lambda(x)\lambda(y | x)$  where  $\lambda(x) \propto \int \lambda(x, y) dy$ . However, there is an extra degree of freedom: we can multiply  $\lambda(x)$  by a positive constant and account for it by multiplying  $\lambda(y | x)$  by its inverse since the intensities need not integrate to one. It is often convenient to choose that constant so that one factor is normalized to be a probability density.

One way to simulate a Poisson process on  $\mathcal{X}$  (and by extension a marked Poisson process on  $\mathcal{X} \times \mathcal{Y}$ ) is to first sample the number of events  $N \sim \text{Po}(\int_{\mathcal{X}} \lambda(x) dx)$ , assuming the integrated intensity is finite, then independently sample the events  $x_n$  according to the probability density  $\frac{\lambda(x)}{\int_{\mathcal{X}} \lambda(x') dx'}$ . The independence in the second step is both a blessing and a curse: it leads to many of the fundamental properties of Poisson processes, like the independence of disjoint subsets, but it precludes more complicated models in which events cluster together.

Neyman-Scott processes [Neyman and Scott, 1958] overcome this limitation by composing two Poisson processes. To simulate a Neyman-Scott process, first sample a set of *latent events*. Each latent event should include a location,  $m_l \in \mathcal{X}$ , where  $\mathcal{X}$  is the same domain as the observed data-points, and a non-negative weight,  $w_l \in \mathbb{R}_+$ . The latent events may also include extra parameters,  $\theta_l \in \Theta$ , which determine the induced impulse response. In a Neyman-Scott process, the latent events are drawn from a marked Poisson process,

$$\{(m_l, w_l, \theta_l)\}_{l=1}^L \sim \text{PP}(\nu(m, w, \theta)), \quad (1)$$

where  $\nu(m, w, \theta) : \mathcal{X} \times \mathbb{R}_+ \times \Theta \rightarrow \mathbb{R}_+$  is an intensity function on the space of locations, weights, and parameters.<sup>1</sup> Without loss of generality, write the intensity as

$$\nu(m, w, \theta) = \bar{L}(\mathcal{X}) p(m, w, \theta) \quad (2)$$

where  $p(m, w, \theta)$  is a normalized probability density and  $\bar{L}(\mathcal{X})$  is the total measure of the domain  $\mathcal{X}$ . Since  $p(m, w, \theta)$  is a normalized probability density, the number of latent events is a Poisson random variable,  $L \sim \text{Po}(\bar{L}(\mathcal{X}))$ .

Each latent event adds a non-negative *impulse response* to the intensity of another marked Poisson pro-

---

<sup>1</sup>Moller and Waagepetersen [2003] refer to this model as a *shot noise Cox process* and reserve the name *Neyman-Scott process* for the special case where the weights are identical and constant.

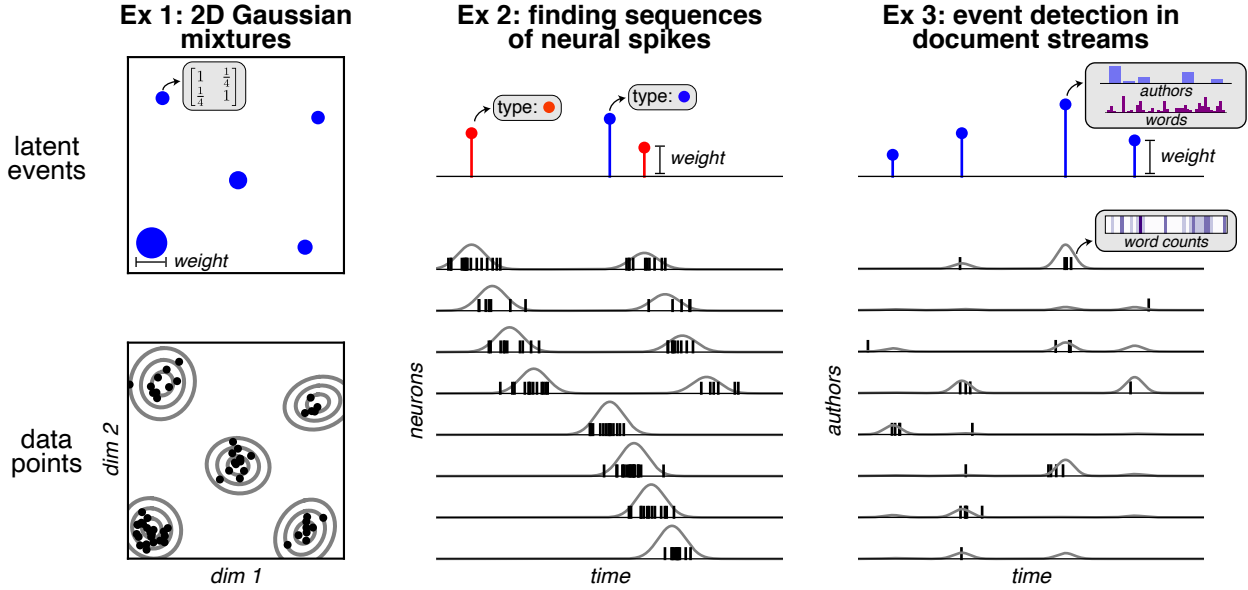


Figure 1: Three example applications of Neyman-Scott processes. Example 1 (left) is a spatial clustering model with Gaussian impulse responses. Each latent event has a location, weight, and a covariance matrix as its parameter (as shown in the gray box, e.g.). The weight determines the expected number of induced data points. Example 2 (middle) is an NSP for finding recurring sequences of spikes in neural recordings. Each latent event has a time, weight, and type (red or blue) as its parameter. The induced data points are spikes with a time and a neuron assignment (i.e. mark). The latent event type determines which neurons participate in the sequence and at what delay. Example 3 (right) is an NSP for detecting events in document streams. Each latent event has a time, weight, and a parameter that specifies the distributions over authors and words. The induced data points are documents with a time, author, and a vector of word counts. In all three examples, goals include inferring latent events, filling in missing data, and predicting data points in unobserved regions of time or space.

cess,

$$\lambda(x, y \mid \{(m_l, w_l, \theta_l)\}_{l=1}^L) = \sum_{l=1}^L w_l p(x, y \mid m_l, \theta_l). \quad (3)$$

As above, assume  $p(x, y \mid m_l, \theta_l)$  is a probability density on  $\mathcal{X} \times \mathcal{Y}$ . Any dependencies between the weights, locations, and parameters can be incorporated into the latent event intensity function  $\nu(m, w, \theta)$ .

Finally, sample the observed data-points from a marked Poisson process,

$$\{(x_n, y_n)\}_{n=1}^N \sim \text{PP}(\lambda(x, y \mid \{(m_l, w_l, \theta_l)\}_{l=1}^L)). \quad (4)$$

Note that the intensity of this Poisson process is itself a stochastic process since it is determined by the random set of latent events and their impulse responses. Therefore, Neyman-Scott processes are a type of *doubly stochastic process* or *Cox process* [Cox, 1955], a class that includes other well-known point process models like the Log Gaussian Cox Process [Møller et al., 1998].

## 2.1 Example applications of Neyman-Scott processes

Neyman-Scott processes are applicable to a wide variety of spatiotemporal clustering problems. Consider the following simple example of spatial clustering with anisotropic Gaussian distributions, which has been used for modeling plant locations in forestry and ecology [Stoyan and Penttinen, 2000, Wiegand and Moloney, 2013].

**Example 1: Spatial clustering with anisotropic Gaussian impulse responses.** Let  $\mathcal{X} \subset \mathbb{R}^2$  denote a compact subset of the 2-dimensional plane, like the square shown in Figure 1 (left). The latent events are uniformly distributed points in  $\mathcal{X}$ , each with non-negative weight. Their parameters are positive definite matrices that determine the covariance of a Gaussian impulse response. The data are points  $x_n \in \mathcal{X}$ , and they do not have marks in this example. In the notation of equations (2) and (3),

$$\bar{L}(\mathcal{X}) = \bar{\nu}|\mathcal{X}| \quad (5)$$

$$p(m, w, \theta) = \text{Unif}(m | \mathcal{X}) \text{Ga}(w | \alpha, \beta) \text{IW}(\theta | d, \Psi) \quad (6)$$

$$p(x | m_l, \theta_l) = \mathcal{N}(x | m_l, \theta_l) \quad (7)$$

where  $\bar{\nu}$  specifies the rate of latent events,  $|\mathcal{X}|$  is the Lebesgue measure of  $\mathcal{X}$ ,  $\text{Ga}(\cdot | \alpha, \beta)$  denotes a gamma density with shape  $\alpha$  and rate  $\beta$  and  $\text{IW}(\cdot | d, \Psi)$  denotes an inverse Wishart density with  $d$  degrees-of-freedom and scale matrix  $\Psi$ . A draw from this model is shown in Figure 1.

This example model generalizes the Thomas process [Thomas, 1949], a Neyman-Scott process in which the locations follow a homogeneous Poisson process on  $\mathcal{X}$  with constant intensity  $\bar{\nu}$ , the weights are identical and constant, and the covariances are isotropic. The Thomas process is nicely tractable: many second-order statistics can be computed in closed form, allowing for parameter estimation via minimum contrast estimation [Møller and Waagepetersen, 2003, Diggle, 2013, Tanaka et al., 2008]. Next we consider a more complex example with marked data points.

**Example 2: Detecting sequences of spikes in neural recordings.** With multielectrode arrays, neuroscientists can record the times at which individual neurons fire action potentials, or *spikes*. A sequence of spike times from one or more neurons is called a *spike train*. We can model a spike train as a collection of tuples  $\{(x_n, y_n)\}_{n=1}^N$  where  $x_n \in \mathcal{X} = [0, T]$  denotes the time of the  $n$ -th spike and  $y_n \in \mathcal{Y} = \{1, \dots, Y\}$  denotes the index of the neuron on which it occurred. An important problem in neuroscience is detecting sequences of spikes that unfold across multiple neurons and recur many times over the course of a recording [Abeles and Gat, 2001, Russo and Durstewitz, 2017, Quaglio et al., 2018].

Consider the following Neyman-Scott process model for sequence detection, as described by Williams et al. [2020b]. Each sequence corresponds to a latent event, which consists of a time (i.e. location)  $m_l \in [0, T]$ , weight  $w_l \in \mathbb{R}_+$ , and a discrete type (i.e. parameter)  $\theta_l \in \{1, \dots, S\}$ . The hyperparameter  $S$  specifies the number of sequence types. In the notation of equations (2) and (3),

we assume,

$$\bar{L}(\mathcal{X}) = \bar{\nu}T \quad (8)$$

$$p(m, w, \theta) = \text{Unif}(m \mid [0, T]) \cdot \text{Ga}(w \mid \alpha, \beta) \cdot \text{Cat}(\theta \mid \pi) \quad (9)$$

$$p(x, y \mid m_l, \theta_l) = \text{Cat}(y \mid a_{\theta_l}) \cdot \mathcal{N}(x \mid m_l + b_{y, \theta_l}, \sigma_{y, \theta_l}^2), \quad (10)$$

The parameter  $\pi \in \Delta_S$  is a distribution over sequence types,  $a_s \in \Delta_Y$  is a distribution over neurons for spikes in sequences of type  $s$ , and  $b_{y,s} \in \mathbb{R}$  and  $\sigma_{y,s} \in \mathbb{R}_+$  specify the latency and width, respectively, of impulse responses induced on neuron  $y$  by latent events of type  $s$ . By varying the offsets, a single latent event can induce a sequence of spikes across a set of neurons, and different sequence types can engage different subsets of neurons, as shown in Figure 1 (middle).

Finally, consider the following example of a Neyman-Scott process for event detection in document streams. The model is similar to the preceding example, but here the latent events and data points each have high-dimensional marks: distributions over words and vectors of word counts, respectively.

**Example 3: Detecting world events from streams of news documents.** Suppose we have a collection of documents, each with a timestamp, author, and a string of words. For example, in political science, we may be interested in discovering structure in diplomatic cables exchanged between multiple countries. We represent the dataset as  $\{(x_n, y_n)\}_{n=1}^N$  where  $x_n \in \mathcal{X} = [0, T]$  denotes the time stamp. The mark is another tuple  $y_n = (y_n^{(a)}, y_n^{(c)})$ , where  $y_n^{(a)} \in \{1, \dots, A\}$  denotes the index of the document’s author and  $y_n^{(c)} \in \mathbb{N}_0^V$  denotes a vector of word counts for each term in a vocabulary of size  $V$ . The idea is that documents that were written around the same time are likely to use similar terms if they are discussing the same recent event. For example, we might see a flurry of diplomatic cables following an election. In many cases, those events are latent and we aim to infer them from the observed documents.

To perform event detection with a Neyman-Scott process, let the latent events of the NSP consist of a time (i.e. location)  $m_l \in [0, T]$ , weight  $w_l \in \mathbb{R}_+$ , and parameters  $\theta_l = (\theta_l^{(a)}, \theta_l^{(c)})$ . The first parameter,  $\theta_l^{(a)} \in \Delta_A$ , is a distribution over authors; the second,  $\theta_l^{(c)} \in \mathbb{R}_+^V$ , is a vector of intensities for each word in the vocabulary. In the notation of equations (2) and (3), we assume,

$$\bar{L}(\mathcal{X}) = \bar{\nu}T$$

$$p(m, w, \theta) = \text{Unif}(m \mid [0, T]) \cdot \text{Ga}(w \mid \alpha, \beta) \cdot \text{Dir}(\theta^{(a)} \mid \alpha_a) \prod_{v=1}^V \text{Ga}(\theta_v^{(c)} \mid \alpha_c, \beta_c)$$

$$p(x, y \mid m_l, \theta) = \mathcal{N}(x \mid m_l, \sigma^2) \cdot \text{Cat}(y^{(a)} \mid \theta_l^{(a)}) \prod_{v=1}^V \text{Po}(y_v^{(c)} \mid \theta_{l,v}^{(c)}).$$

where  $\bar{\nu}$  specifies the rate of latent events,  $\alpha_a$  is the concentration parameter of the author distribution,  $\alpha_c$  and  $\beta_c$  are the concentration and rate parameters of the word intensity distribution, and  $\sigma$  effectively determines duration of the latent event.

These examples bear strong resemblance to mixture models, with each latent event corresponding to a cluster. The *Poisson superposition principle* [Kingman, 1992] makes this connection explicit. Note that given the set of latent events, the intensity function in eq. (3) is a sum of non-negative impulse

---

**Algorithm 1:** Sample an NSP

---

```
sample:  $L \sim \text{Po}(\bar{L}(\mathcal{X}))$ 
for  $l = 1, \dots, L$  do
  sample:  $m_l, w_l, \theta_l \sim p(m, w, \theta)$ 
  sample:  $N_l \sim \text{Po}(w_l)$ 
  for  $n = 1, \dots, N_l$  do
    sample:
       $x_{l,n}, y_{l,n} \sim p(x, y \mid m_l, \theta_l)$ 
  end
end
return  $\cup_{l=1}^L \{(x_{l,n}, y_{l,n})\}_{n=1}^{N_l}$ 
```

---

---

**Algorithm 2:** Sample an NSP (v2)

---

```
sample:  $L \sim \text{Po}(\bar{L}(\mathcal{X}))$ 
for  $l = 1, \dots, L$  do
  sample:  $m_l, w_l, \theta_l \sim p(m, w, \theta)$ 
end
set:  $W = \sum_{l=1}^L w_l$ 
set:  $\pi = (w_1/W, \dots, w_L/W)$ 
sample:  $N \sim \text{Po}(W)$ 
for  $n = 1, \dots, N$  do
  sample:  $z_n \sim \text{Cat}(\pi)$ 
  sample:  $x_n \sim p(x \mid m_{z_n}, \theta_{z_n})$ 
end
return  $\{x_n\}_{n=1}^N$ 
```

---

responses. The superposition principle says that we can sample such a Poisson process by independently sampling data points from Poisson processes for each impulse response and taking their union.

To sample data points for each impulse response, recall the two-step procedure from above: first sample the number of data points, then sample their locations and marks independently according to the normalized impulse response. Since the impulse responses are weighted probability density functions, the expected number of induced data points is simply the weight,  $w_l$ , and the normalized impulse responses are simply the conditional densities,  $p(x, y \mid m_l, \theta_l)$ . This procedure for sampling a NSP is shown in Algorithm 1.

This sampling procedure lets us interpret the Neyman-Scott process as a clustering model in which each data-point is attributed to one of the underlying latent events. Moreover, under the NSP, the number of clusters  $L$  is a random variable, suggesting a connection between Neyman-Scott processes and Bayesian nonparametric mixture models. We formalize this relationship in the next section.

### 3 Neyman-Scott Processes & Bayesian Nonparametric Mixture Models

Our first contribution is to establish a connection between Neyman-Scott processes, Dirichlet process mixture models (DPMMs) [Antoniak, 1974, Lo, 1984, Neal, 1992, Escobar and West, 1995], and the mixture of finite mixture model (MFMM) recently studied by Miller and Harrison [2018]. MFMMs are Bayesian mixture models in which the number of clusters is a finite random variable. We will show how the NSP can be seen as an MFMM in which the distribution of the number of components depends on how many data points are observed. This relationship allows us to extend many of the results of Miller and Harrison [2018] and characterize the NSP in terms of its random partition distribution, urn scheme, and random measure formulation. In doing so, we will see that the Neyman-Scott Process occupies a privileged place among MFMMs: in a certain limit, the NSP reduces to the classic DPMM. This relationship allows the Neyman-Scott process to interpolate between these two important model classes and inherit the efficient inference algorithms available for DPMMs and MFMMs.

To establish the connection to MFMMs and DPMMs, we first present an equivalent sampling procedure

---

**Algorithm 3:** Sample an NSP with gamma weights

---

```

sample:  $L \sim \text{Po}(\bar{L}(\mathcal{X}))$ 
for  $l = 1, \dots, L$  do
  | sample:  $m_l, \theta_l \sim p(m, \theta)$ 
end
sample:  $W \sim \text{Ga}(L\alpha, \beta)$ 
sample:  $\pi \sim \text{Dir}(\alpha 1_L)$ 
sample:  $N \sim \text{Po}(W)$ 
for  $n = 1, \dots, N$  do
  | sample:  $z_n \sim \text{Cat}(\pi)$ 
  | sample:  $x_n \sim p(x | m_{z_n}, \theta_{z_n})$ 
end
return  $\{x_n\}_{n=1}^N$ 

```

---



---

**Algorithm 4:** Sample an NSP with gamma weights (v2)

---

```

sample:  $L \sim \text{Po}(\bar{L}(\mathcal{X}))$ 
for  $l = 1, \dots, L$  do
  | sample:  $m_l, \theta_l \sim p(m, \theta)$ 
end
sample:  $\pi \sim \text{Dir}(\alpha 1_L)$ 
sample:  $N \sim \text{NB}(L\alpha, (1 + \beta)^{-1})$ 
for  $n = 1, \dots, N$  do
  | sample:  $z_n \sim \text{Cat}(\pi)$ 
  | sample:  $x_n \sim p(x | m_{z_n}, \theta_{z_n})$ 
end
return  $\{x_n\}_{n=1}^N$ 

```

---

for Neyman-Scott processes. Rather than sampling the numbers of induced data points,  $N_l$ , for each of the latent events, we first sample the total number of induced data points,  $N$ , and then assign each data point a *parent* latent event. Since each  $N_l$  is an independent Poisson random variable, the total number of induced data points is also Poisson distributed and the parents are categorical random variables [Kingman, 1992]. The alternative algorithm is shown in Algorithm 2.

The sampling procedure simplifies even further under the following assumption.

**Assumption 1.** *The latent event intensity factors as,*

$$v(m, w, \theta) = \bar{L}(\mathcal{X}) \text{Ga}(w | \alpha, \beta) p(m, \theta). \quad (11)$$

*That is, the latent event weights are gamma random variables with shape  $\alpha$  and inverse scale  $\beta$ , and they are independent of the latent event locations and parameters.*

Under this assumption, the Neyman-Scott process becomes a *shot noise G Cox process* [Brix, 1999, Moller and Waagepetersen, 2003], which in turn generalizes the Poisson-gamma process [Wolpert and Ickstadt, 1998]. We will simply call it an NSP with gamma weights.

The total weight in Algorithm 2 is the sum of independent and identically distributed gamma random variables, which is also a gamma distributed,  $W \sim \text{Ga}(L\alpha, \beta)$ . Moreover, the normalized weights in Algorithm 2 follow a symmetric Dirichlet distribution,  $\pi \sim \text{Dir}(\alpha 1_L)$ , where  $1_L$  is a length- $L$  vector of ones. Thanks to a unique property of the gamma distribution [Lukacs, 1955], the total weight is independent of the normalized weights. Algorithm 3 uses these three properties to sample an NSP with gamma weights, per Assumption 1 above. Finally, since the gamma and Poisson are conjugate, we can marginalize over the total weight to obtain a negative binomial distribution on the number of data points, as in collapsed sampling procedure in Algorithm 4.

Compare Algorithm 4 for sampling an NSP with gamma weights to Algorithm 5 for sampling an MFMM, adapted from Miller and Harrison [2018]. There are three main differences. First, the MFMM allows for arbitrary distributions on the number of components,  $p(L)$ , whereas the NSP has a Poisson distribution. Second, the number of latent events in an NSP depends on the total measure over the domain  $\mathcal{X}$ ; that



is, an NSP can generalize from one domain to another and scale the expected number of latent events accordingly. Third, the MFMM treats the number of observed events  $N$  as fixed, whereas the NSP model treats  $N$  as a random variable that depends on the number of latent events,  $L$ .

Conditioned on the number of data points, however, the Neyman-Scott process with gamma weights is a special case of the mixture of finite mixtures model. In an NSP, the number of data points carries information about the number of latent events—intuitively, more data points suggests more clusters. In particular, given that we have observed  $N$  data points, the NSP with gamma weights is a special case of the MFMM in which  $p(L | N) \propto \text{Po}(L | \bar{L}(\mathcal{X})) \cdot \text{NB}(N | L\alpha, (1 + \beta)^{-1})$ , where NB is the negative binomial probability mass function (pmf). This distribution is closely related to a shifted confluent hypergeometric distribution, which we call the *Schein distribution* after [Schein et al. \[2019\]](#). The Schein distribution is in turn closely related to the Pólya-Aeppli distribution [[Johnson et al., 2005](#)]. Its pmf has a closed-form expression in terms of hypergeometric functions.

The correspondence between NSPs and MFMMs enables many of the results of [Miller and Harrison \[2018\]](#) to be adapted to the Neyman-Scott process. In particular, we will derive the marginal distribution over partitions of  $N$  data points in an NSP and a corresponding Pólya urn scheme, which leads to yet another algorithm for sampling Neyman-Scott processes. This urn scheme will suggest an efficient collapsed Gibbs sampling algorithm for posterior inference in NSPs with gamma weights, which we develop in Section 5. Moreover, the urn scheme will reveal a novel connection between Neyman-Scott processes and Dirichlet process mixture models.

### 3.1 The exchangeable partition distribution of a Neyman-Scott process

The Neyman-Scott process induces a random partition of data points into clusters associated with different latent events. Let  $N$  denote the number of observed data points and  $\mathcal{C}$  denote a partition of the indices  $\{1, \dots, N\}$  induced by the *parent assignments*  $z_n$  in Algorithm 4. In other words,  $\mathcal{C}$  is a set of disjoint, non-empty sets whose union is  $[N] = \{1, \dots, N\}$ . We represent the partition as  $\mathcal{C} = \{\mathcal{C}_k : |\mathcal{C}_k| > 0\}$ , where  $\mathcal{C}_k = \{n : z_n = k\}$  is the set of data indices assigned to latent event  $k$  and  $|\mathcal{C}_k|$  is the size of that cluster. The size of the partition,  $|\mathcal{C}|$ , is the number of latent events that induced at least one observed data point, so we must have  $L \geq |\mathcal{C}|$ .

The parent assignments induce a partition of the observed events, but they are tied to a particular labeling of the latent events. The partition, by contrast, is invariant to permutations of the latent event indices. Working with partitions frees us from keeping track of latent event indices or empty components in mixture models—we only need to infer how the finite number of data points are partitioned into different components.

**Theorem 1.** *Under Assumption 1, the prior probability of the partition induced by an NSP, integrating*

---

**Algorithm 5:** Sample an MFMM with  $N$  data points

---

```

sample:  $L \sim p(L)$ 
for  $l = 1, \dots, L$  do
  | sample:  $m_l, \theta_l \sim p(m, \theta)$ 
end
sample:  $\pi \sim \text{Dir}(\alpha \mathbf{1}_L)$ 
for  $n = 1, \dots, N$  do
  | sample:  $z_n \sim \text{Cat}(\pi)$ 
  | sample:  $x_n \sim p(x | m_{z_n}, \theta_{z_n})$ 
end
return  $\{x_n\}_{n=1}^N$ 

```

---

over the latent event locations, weights, and parameters, is,

$$p(N, \mathcal{C}) = V_{N,|\mathcal{C}|} \prod_{\mathcal{C}_k \in \mathcal{C}} \frac{\Gamma(|\mathcal{C}_k| + \alpha)}{\Gamma(\alpha)}, \quad (12)$$

where  $\alpha$  and  $\beta$  are the shape and rate, respectively, of the gamma prior on latent event weights,  $|\mathcal{C}|$  is the number of clusters in the partition,  $|\mathcal{C}_k|$  is the size of the  $k$ -th cluster in the partition,  $N = \sum_{\mathcal{C}_k \in \mathcal{C}} |\mathcal{C}_k|$  is the total number of data points (a random variable), and

$$V_{N,|\mathcal{C}|} = \frac{1}{N!} \left( \frac{1}{1 + \beta} \right)^N \sum_{L=|\mathcal{C}|}^{\infty} \text{Po}(L | \bar{L}(\mathcal{X})) \frac{L!}{(L - |\mathcal{C}|)!} \left( \frac{\beta}{1 + \beta} \right)^{L\alpha}. \quad (13)$$

Theorem 1 and its proof (given in Appendix A) closely parallel the main theorem of [Miller and Harrison \[2018\]](#), which gives the partition distribution for mixture of finite mixture models. The main difference is that eq. 12 is a distribution on partitions of random size  $N \in \mathbb{N}_0$ . To obtain a conditional distribution  $p(\mathcal{C} | N)$  on partitions of given size  $N$ —the partition distribution more commonly considered [[Pitman, 2006](#), [Miller and Harrison, 2018](#)]  
—we need to divide by the probability of obtaining  $N$  data points,

$$p(N) = \sum_{L=0}^{\infty} \text{Po}(L | \bar{L}(\mathcal{X})) \text{NB}(N | L\alpha, (1 + \beta)^{-1}). \quad (14)$$

The distribution above is a Poisson-mixed negative binomial. It does not, to our knowledge, have an analytical form, but we will not need one for our purposes.

Note that  $p(\mathcal{C} | N)$  is a symmetric function of the cluster sizes,  $|\mathcal{C}_k|$ , and therefore it is invariant to permutations of the integers  $[N]$ . Thus,  $\mathcal{C}$  is an *exchangeable* random partition and  $p(\mathcal{C} | N)$  is an exchangeable partition probability function (EPPF) [[Pitman, 2006](#)]. In particular, it takes the form of a Gibbs partition [[Gnedin and Pitman, 2006](#)] since it factors into a term that depends on the number of data points and clusters ( $V_{N,|\mathcal{C}|}/p(N)$ ) and a product of rising factorials ( $\Gamma(|\mathcal{C}_k| + \alpha)/\Gamma(\alpha)$ ) depending on the size of each cluster.

The EPPF offers yet another way of sampling a Neyman-Scott process as shown in Algorithm 6. First sample a random partition  $\mathcal{C}$ , which specifies the number of data points; then sample parameters for each cluster in the partition; and finally, independently sample data points for each cluster. The key step is sampling a random partition, and as we will see in the next section, this can be done with a simple Pólya-urn process. The main advantage of this formulation is that it only involves the partition, cluster parameters, and data points, and that enables the simple collapsed Gibbs sampling algorithm for NSPs presented in Section 5.

### 3.2 Connecting Neyman-Scott processes and Dirichlet process mixture models

Like the MFMM and other nonparametric mixture models, the Neyman-Scott process can be characterized by its Pólya-urn scheme (aka “restaurant process”). A Pólya-urn scheme is a discrete-time Markov process on partitions of the integers. Indices  $n = 1, 2, \dots$  are introduced one at a time, and they are either added to an existing cluster or to a new, singleton cluster. The Blackwell-MacQueen urn scheme [[Blackwell and MacQueen, 1973](#)] (aka “Chinese restaurant process”) and Pitman-Yor process [[Pitman and Yor,](#)

---

**Algorithm 6:** Sample an NSP with gamma weights (v3)

---

**sample:**  $N, \mathcal{C} \sim p(N, \mathcal{C})$   
**for**  $\mathcal{C}_k \in \mathcal{C}$  **do**  
    **sample:**  $m_k, \theta_k \sim p(m, \theta)$   
    **for**  $n \in \mathcal{C}_k$  **do**  
        **sample:**  
             $x_n, y_n \sim p(x, y \mid m_k, \theta_k)$   
    **end**  
**end**  
**return**  $\{(x_n, y_n)\}_{n=1}^N$

---



---

**Algorithm 7:** Sample an NSP partition  $N, \mathcal{C} \sim p(N, \mathcal{C})$

---

**sample:**  $\tilde{L} \sim \text{Po}(\bar{\nu} \mid \mathcal{X})$   
**sample:**  $N \sim \text{NB}(\tilde{L}\alpha, (1 + \beta)^{-1})$   
**set:**  $\mathcal{C}_1 = \{1\}$  and  $\mathcal{C} = \{\mathcal{C}_1\}$   
**for**  $n = 2, \dots, N$  **do**  
    **set:**  $Z = n - 1 + |\mathcal{C}| \alpha + \alpha \bar{L}(\mathcal{X}) \left(\frac{\beta}{1 + \beta}\right)^\alpha$   
    **set:** index  $n$  in:  
    a.  $\mathcal{C}_k \in \mathcal{C}$  w/pr  $\frac{|\mathcal{C}_k| + \alpha}{Z}$   
    b. new cluster w/pr  $\frac{\alpha \bar{L}(\mathcal{X}) \left(\frac{\beta}{1 + \beta}\right)^\alpha}{Z}$   
**end**  
**return**  $N, \mathcal{C}$

---

1997] are classic examples. We will show that the Neyman-Scott process corresponds to an urn scheme of a very similar nature, and, like the two-parameter Pitman-Yor process, it subsumes the Blackwell-MacQueen urn scheme as a limiting case.

The following corollary describes an urn scheme in which the marginal distribution after  $N$  steps is  $p(\mathcal{C} \mid N)$ .

**Theorem 2.** *Let  $\mathcal{C}'$  be a partition of the integers  $[N-1]$ . The following transition operator is a distribution on partitions  $\mathcal{C}$  of the integers  $[N]$  that equal  $\mathcal{C}'$  when the integer  $N$  is removed.*

$$p(\mathcal{C} \mid \mathcal{C}') \propto \begin{cases} |\mathcal{C}_k| + \alpha & \text{if } \mathcal{C}_k \in \mathcal{C}' \text{ and } \mathcal{C}_k \cup \{N\} \in \mathcal{C} \\ \alpha \frac{V_{N, |\mathcal{C}'|+1}}{V_{N, |\mathcal{C}'|}} & \text{if } N \text{ is a singleton; i.e. } \{N\} \in \mathcal{C} \end{cases} \quad (15)$$

Starting with  $\mathcal{C} = \{\{1\}\}$  and applying this transition operator  $N - 1$  times yields a partition  $\mathcal{C}$  of the integers  $[N]$  that is distributed according to  $p(\mathcal{C} \mid N)$ .

Theorem 2 is equivalent to Theorem 4.1 of Miller and Harrison [2018] for mixture of finite mixture models, which is unsurprising since we have already shown that Neyman-Scott processes are special cases of MFMMs when conditioned on the number of data points.

Here is where the Neyman-Scott process distinguishes itself from other mixture of finite mixture models. In the NSP, the ratio  $V_{N, |\mathcal{C}'|+1} / V_{N, |\mathcal{C}'|}$  is a constant determined only by the latent event intensity and the parameters of the weight distribution.

**Lemma 1.** *Under a Neyman-Scott process satisfying Assumption 1,*

$$\frac{V_{N, |\mathcal{C}'|+1}}{V_{N, |\mathcal{C}'|}} = \bar{L}(\mathcal{X}) \left(\frac{\beta}{1 + \beta}\right)^\alpha. \quad (16)$$

The proof of this lemma follows from simple substitution, as shown in Appendix A. This ratio controls the probability of adding a new cluster in the urn process described in Theorem 2. In general MFMMs, the ratio changes as a function of  $|\mathcal{C}'|$  and  $N$ , and Miller and Harrison [2018] recommend precomputing it for a range of values. For Neyman-Scott processes with gamma weights, it is simply a constant.

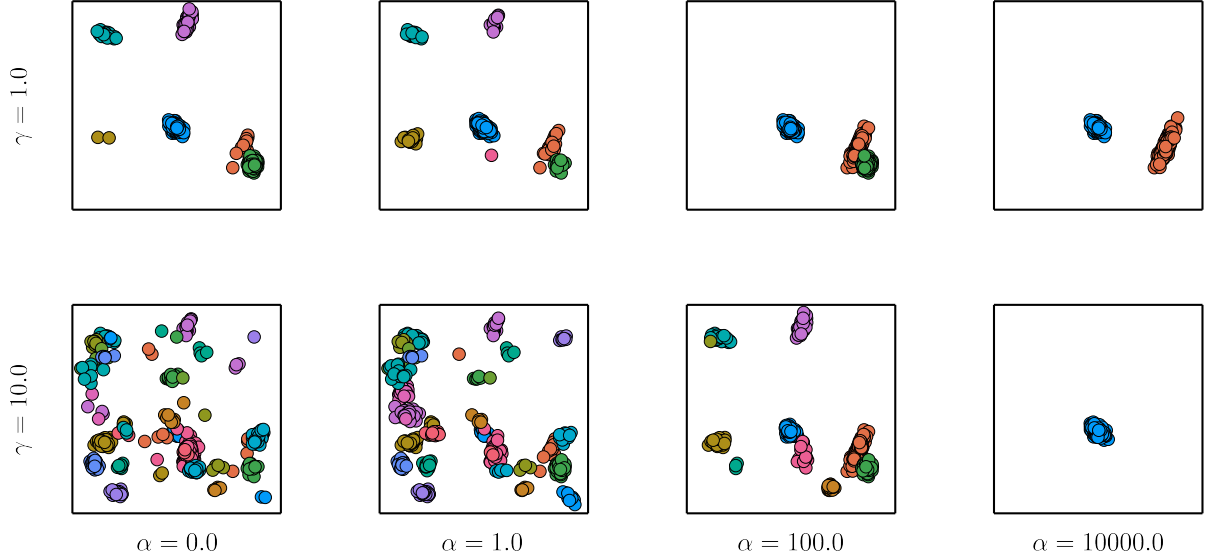


Figure 2: Neyman-Scott processes with gamma weights contain Dirichlet process mixture models as a limiting case. Each panel shows  $N = 100$  data points drawn from a 2D Neyman-Scott processes with gamma weights and Gaussian clusters (Example 1). Here,  $\mathcal{X} = [0, 1]^2$ ,  $\bar{L}(\mathcal{X}) = \bar{\nu}$ ,  $p(m) = \text{Unif}(m \mid \mathcal{X})$ , and  $\beta = 2$ . The shape  $\alpha$  of the latent event weights varies between 0 and 10,000, and the concentration  $\gamma$  is set to 1 (top row) or 10 (bottom row). The latent event intensity  $\bar{\nu}$  is set so that  $\gamma = \bar{\nu}\alpha^{(\beta/1+\beta)^\alpha}$ . When  $\alpha = 0$ , the data is drawn from a Dirichlet process mixture model with concentration  $\gamma$ .

Lemma 1 also hints at a close relationship between NSPs and Dirichlet process mixture models. Recall that in the Blackwell-MacQueen urn scheme that generates partitions of Dirichlet process mixture model, the probability of adding a new cluster is also constant [Blackwell and MacQueen, 1973]. Specifically, the probability of adding to an existing cluster is proportional to the size of the cluster,  $|\mathcal{C}_k|$ , and the probability of creating a new cluster is proportional to a constant  $\gamma$ , the Dirichlet process concentration. The following corollary formalizes this relationship, showing how the DPMM arises when as a limiting case of the NSP with infinitely many latent events with weights that are almost surely zero.

**Corollary 3.** *The Neyman-Scott process with gamma weights (Assumption 1) approaches a Dirichlet process mixture model with concentration  $\gamma$  and a base measure with density  $p(m, \theta)$  in the limit that  $\alpha \rightarrow 0$  while  $\alpha \bar{L}(\mathcal{X}) \rightarrow \gamma$ .*

*Proof.* In this limit, the probability of adding a new cluster is  $\lim_{\alpha \rightarrow 0} \alpha \bar{L}(\mathcal{X})^{(\beta/1+\beta)^\alpha} = \gamma$  and the probability of adding to an existing cluster is  $\lim_{\alpha \rightarrow 0} |\mathcal{C}_k| + \alpha = |\mathcal{C}_k|$ . Thus, the urn scheme given in Theorem 2 converges to the Blackwell-MacQueen urn scheme, which underlies the Dirichlet process mixture model. The cluster parameters in the NSP are sampled i.i.d. from  $p(m, \theta)$  in the same way cluster parameters are sampled independently from the base measure in a DPMM.  $\square$

Figure 2 shows realizations of the NSP urn scheme for  $N = 100$  data points. In each row, the shape parameter  $\alpha$  is varied while the inverse scale  $\beta$  is fixed and the latent event rate  $\bar{\nu}$  is changed so that  $\gamma = \bar{\nu}\alpha^{(\beta/1+\beta)^\alpha}$  is held constant. In the limit where  $\alpha \rightarrow 0$  (i.e. in the left-most column), the urn process

is identical to the Blackwell-MacQueen urn process for Dirichlet process mixture models, as stated in Corollary 3. As the shape parameter  $\alpha$  is increased, there is a greater tendency to add data points to existing clusters, leading to fewer clusters for a fixed dataset size. The DPMM limit, in contrast, has a larger number of small clusters.

The Neyman-Scott urn scheme in Theorem 2 is even more similar to the urn scheme of the two-parameter Pitman-Yor process [Pitman and Yor, 1997]. The Pitman-Yor scheme adds indices to existing clusters with probability proportional to  $|\mathcal{C}_k| - \delta$  and to a new cluster with probability proportional to  $\gamma + |\mathcal{C}|\delta$ . When the *discount* parameter  $\delta$  is zero, the Pitman-Yor process is also equivalent to the Dirichlet process (and its urn scheme is equivalent to the Blackwell-MacQueen urn scheme). When the discount parameter is negative, the Pitman-Yor urn scheme preferentially adds to existing clusters, just like in the NSP urn scheme, suggesting a correspondence between the shape parameter  $\alpha$  in the NSP and  $-\delta$  in the Pitman-Yor scheme. However, when  $\delta < 0$ , the *strength* parameter  $\gamma$  must equal  $L|\delta|$  for integer  $L$  so that the probability of creating a new cluster equals exactly zero once  $|\mathcal{C}| = L$ . In this case the Pitman-Yor process generates a partition for a finite Dirichlet-multinomial model. That is where the Neyman-Scott and Pitman-Yor urn schemes differ: in the NSP, the probability of creating a new cluster is proportional to a constant, regardless of the number of existing clusters; in the Pitman-Yor urn scheme with a negative discount factor, that probability decreases as the number of clusters increases. Both the Neyman-Scott and Pitman-Yor urn schemes converge to the Blackwell-MacQueen urn scheme under certain limits, but they differ in their approach.

The connection between Neyman-Scott processes and Dirichlet process mixture models is also evident from their random measures. We can view the latent events of the NSP as a discrete random measure on  $\mathcal{X} \times \theta$  with a Poisson-distributed number of atoms. The  $l$ -th atom is located at  $(m_l, \theta_l)$  and has weight  $w_l$ . Intuitively, in the limit described in Corollary 3, the number of atoms goes to infinity and the weights go to zero. In this limit, the random measure approaches a gamma process that, once normalized, yields a Dirichlet process. The induced intensity arises by convolving this random measure with an impulse response to obtain the intensity  $\lambda(x, y | \{(m_l, w_l, \theta_l)\}_{l=1}^L)$ . Normalizing the intensity yields the mixture density of a DPMM. We formalize this random measure perspective in Appendix B.

## 4 Accounting for Background Data Points

Often, the observed data points naturally separate into those induced by latent events and those that are “background noise.” One way to account for such background events is by adding an extra term to the intensity function that produces the observed data points,

$$\lambda(x, y | \{(m_l, w_l, \theta_l)\}_{l=1}^L) = \lambda_0(x, y) + \sum_{l=1}^L w_l p(x | m_l, \theta_l) \quad (17)$$

where  $\lambda_0(x, y) : \mathcal{X} \times \mathcal{Y} \rightarrow \mathbb{R}_+$  is a non-negative intensity function. Then, the Neyman-Scott process sampling procedure (Algorithm 1) has one extra step of sampling background data points  $\{(x_{0,n}, y_{0,n})\}_{n=1}^{N_0} \sim \text{PP}(\lambda_0(x))$ . The complete set of data points,  $\cup_{l=0}^L \{(x_{l,n}, y_{l,n})\}_{n=1}^{N_l}$ , is the union of the background data points and those induced by latent events.

There are a few ways of modeling the background intensity. Without loss of generality, factor the intensity as  $\lambda_0(x, y) = \lambda_0(x)p(y | x)$ , where  $p(y | x)$  is a normalized probability density on  $\mathcal{Y}$ . We will

primarily focus on the spatiotemporal intensity  $\lambda_0(x)$  and assume the mark density  $p(y | x)$  is easy to model. The simplest background model is a constant, homogeneous intensity,  $\lambda_0(x) = \bar{\lambda}_0$ . Under this model, the induced data points are superimposed on top of a background of uniformly distributed data points, and the number of background data points is determined by  $\bar{\lambda}_0$ . Alternatively,  $\lambda_0(x)$  could be modeled with a general, nonparametric model like a log Gaussian Cox process [Møller et al., 1998] or sigmoidal Gaussian Cox process [Adams et al., 2009]. With such models, we can incorporate any spatiotemporal covariates into the prior distribution on background intensities. Our only requirements are that we must be able to evaluate the background intensity at any point  $(x, y)$  and the posterior distribution over background intensities given background data points be amenable to MCMC sampling. It is important to note that there is a risk of non-identifiability with general parametric background intensities. If the background intensity can subsume the impulse responses, then there is no way to distinguish between background and induced data points. A simple and often intuitive solution to this problem is to assume that the background intensity varies slowly relative to the impulse responses; i.e. to assume a separation of spatiotemporal scales.

Regardless of the background model, the Neyman-Scott process with an additive background intensity and gamma weights also admits a simple partition distribution. Let  $\mathcal{C}_0 \subseteq [N]$  denote the subset of indices assigned to the background and  $\mathcal{C}$  be a partition of  $[N] \setminus \mathcal{C}_0$ .

**Theorem 4.** *Under Assumption 1, the prior probability of the partition induced by an NSP with a background intensity  $\lambda_0(x)$ , integrating over the latent event locations, weights, and parameters, is,*

$$p(N, \mathcal{C}_0, \mathcal{C}) = \left( \frac{(N - |\mathcal{C}_0|)!}{N!} e^{-w_0(\mathcal{X})} w_0(\mathcal{X})^{|\mathcal{C}_0|} \right) V_{N-|\mathcal{C}_0|, |\mathcal{C}|} \prod_{\mathcal{C}_k \in \mathcal{C}} \frac{\Gamma(|\mathcal{C}_k| + \alpha)}{\Gamma(\alpha)}, \quad (18)$$

where  $\alpha$  and  $\beta$  are the shape and rate, respectively, of the gamma prior on weights,  $|\mathcal{C}|$  is the number of clusters in the partition,  $|\mathcal{C}_k|$  is the size of the  $k$ -th cluster in the partition,  $N = |\mathcal{C}_0| + \sum_{\mathcal{C}_k \in \mathcal{C}} |\mathcal{C}_k|$  is the total number of data points (a random variable), and where  $w_0(\mathcal{X}) = \int_{\mathcal{X}} \lambda_0(x) dx$  is the integrated background intensity.

A partition of size  $N$  can be generated recursively with the following urn scheme,

$$p(\mathcal{C}_0, \mathcal{C} | \mathcal{C}'_0, \mathcal{C}') \propto \begin{cases} w_0(\mathcal{X})(1 + \beta) & \text{if } \mathcal{C}_0 = \mathcal{C}'_0 \cup \{N\} \text{ and } \mathcal{C} = \mathcal{C}' \\ |\mathcal{C}'_k| + \alpha & \text{if } \mathcal{C}'_k \in \mathcal{C}' \text{ and } \mathcal{C}'_k \cup \{N\} \in \mathcal{C} \\ \alpha \bar{L}(\mathcal{X}) \left( \frac{\beta}{1+\beta} \right)^\alpha & \text{if } N \text{ is a singleton; i.e. } \{N\} \in \mathcal{C} \end{cases} \quad (19)$$

where  $\{\mathcal{C}'_0\} \cup \mathcal{C}'$  is a partition of the integers  $[N-1]$  and  $\{\mathcal{C}_0\} \cup \mathcal{C}$  is a partition of  $[N]$  obtained by adding index  $N$  as described above.

Theorem 4 closely parallels Theorems 1 and 2, as does its proof (given in Appendix A). The only difference is that here we separate the background indices,  $\mathcal{C}_0$ , from the partition of the remaining indices,  $\mathcal{C}$ . In the terminology of Pitman [2006], eq. (18), once normalized by  $p(N)$ , is a *partially* exchangeable partition probability function since it is not symmetric in the cluster indices; the background cluster is treated differently.

---

**Algorithm 8:** Collapsed Gibbs sampling for Neyman-Scott processes with gamma weights

---

**Input:** Data points  $\{(x_n, y_n)\}_{n=1}^N$ , hyperparameters  $\alpha, \beta, \bar{L}(\mathcal{X})$

Initialize all data points to the background:  $\mathcal{C}_0 = \{1, \dots, N\}$  and  $\mathcal{C} = \{\}$ .

**repeat**  $S$  times to draw  $S$  samples

1. Sample parent assignments, integrating over latent events:  
  **for**  $n = 1, \dots, N$ , remove  $n$  from its current cluster and place it in...
  - a. the background cluster,  $\mathcal{C}_0$ , with probability  $\propto \lambda_0(x_n, y_n)(1 + \beta)$
  - b. cluster  $\mathcal{C}_k$ , with probability  $\propto (|\mathcal{C}_k| + \alpha) p(x_n, y_n \mid \{(x_{n'}, y_{n'}) : n' \in \mathcal{C}_k\})$
  - c. a new cluster with probability  $\propto \alpha \bar{L}(\mathcal{X}) \left(\frac{\beta}{1+\beta}\right)^\alpha p(x_n, y_n)$**end**
2. Sample background intensity given the data points  $\{(x_n, y_n) : n \in \mathcal{C}_0\}$ .
3. Sample latent events:  
  **for**  $\mathcal{C}_k \in \mathcal{C}$ :  
    Sample locations and parameters  $m_k, \theta_k \sim p(m_k, \theta_k \mid \{(x_n, y_n) : n \in \mathcal{C}_k\})$   
    Sample weights  $w_k \sim \text{Ga}(\alpha + |\mathcal{C}_k|, \beta + 1)$   
  **end**
4. [Optionally] Sample hyperparameters:  
  Sample hyperparameters of  $p(m, \theta)$  given the samples  $\{(m_k, \theta_k)\}$   
  Sample number of empty clusters  $E \sim \text{Po}\left(\bar{L}(\mathcal{X}) \left(\frac{\beta}{1+\beta}\right)^\alpha\right)$ . Set  $L = |\mathcal{C}| + E$ .  
  Sample homogenous latent event intensity  $\bar{\nu} \sim \text{Ga}(\alpha_\nu + L, \beta_\nu + |\mathcal{X}|)$   
  Sample weights for empty clusters  $w_l \sim \text{Ga}(\alpha, \beta + 1)$  for  $l = |\mathcal{C}| + 1, \dots, L$   
  Sample hyperparameters  $p(\alpha, \beta \mid \{w_l\}_{l=1}^L) \propto p(\alpha, \beta) \prod_{l=1}^L \text{Ga}(w_l \mid \alpha, \beta)$

**end**

---

## 5 Bayesian Learning and Inference for Neyman-Scott Processes

Having shown the relationship between Neyman-Scott processes with gamma weights, mixture of finite mixture models, and Dirichlet process mixture models, we can adapt standard collapsed Gibbs sampling algorithms for MFMMs [Miller and Harrison, 2018] and DPMMs [MacEachern, 1994, Neal, 2000] to NSPs. The resulting algorithm is quite different from existing inference algorithms for NSPs. Rather than proposing to add or remove latent events, as in reversible jump MCMC algorithms [Moller and Waagepetersen, 2003, Møller and Toftaker, 2014], the collapsed Gibbs algorithm marginalizes over latent event locations and parameters and operates directly on the posterior over partitions. Unlike minimum contrast estimation methods, the collapsed Gibbs algorithm asymptotically generates samples from the posterior distribution and makes minimal assumptions about the latent events and their impulse responses.

Algorithm 8 assumes access to the marginal likelihood,

$$p(x_n, y_n) = \int p(x_n, y_n \mid m, \theta) p(m, \theta) dm d\theta \quad (20)$$

and the predictive likelihood

$$p(x_n, y_n \mid \{(x_{n'}, y_{n'}) : n' \in \mathcal{C}_k\}) = \int p(x_n, y_n \mid m, \theta) p(m, \theta \mid \{(x_{n'}, y_{n'}) : n' \in \mathcal{C}_k\}) dm d\theta. \quad (21)$$

Closed-form expressions for these likelihoods are available for conjugate exponential family models, in which case they depend only on prior and posterior sufficient statistics. However, the same extensions that have been developed for collapsed Gibbs sampling in DPMMs and MFMMs apply for the nonconjugate case. If the marginal likelihood in eq. (20) is not available in closed form, auxiliary variable methods like Algorithm 8 of Neal [2000] may be used. Likewise, split-merge methods [Jain and Neal, 2004, 2007] can improve the mixing time of the sampling algorithm with larger updates to the partition.

**Sampling the background intensity** After sampling the partition, we update the background intensity given the data points assigned to the background cluster,  $\{x_n : n \in \mathcal{C}_0\}$ . We assume access to MCMC transition operators that leave the conditional distribution,  $p(\lambda_0(x) \mid \{x_n : n \in \mathcal{C}_0\})$ , invariant. For the simple, homogenous background intensity model with a gamma prior  $\bar{\lambda}_0 \sim \text{Ga}(\alpha_0, \beta_0)$ , the conditional distribution of  $\bar{\lambda}_0$  is available in closed form,

$$p(\bar{\lambda}_0 \mid \{x_n : n \in \mathcal{C}_0\}) = \text{Ga}(\bar{\lambda}_0 \mid \alpha_0 + |\mathcal{C}_0|, \beta_0 + |\mathcal{X}|). \quad (22)$$

**Sampling the latent events** Given the partition and global parameters, it is straightforward to sample the latent events. We update the latent event parameters by sampling  $p(m_k, \theta_k \mid \{x_n : n \in \mathcal{C}_k\})$  for each cluster. If  $p(m, \theta)$  in the latent event intensity has any parameters, they can be updated given the samples  $\{(m_k, \theta_k)\}_{k=1}^{|\mathcal{C}|}$ . In our three examples,  $p(m, \theta)$  is an exponential family density, so we place a conjugate prior on its parameters to enable simple Gibbs updates. Otherwise, the parameter estimates are only for visualization purposes; they are immediately discarded before the subsequent partition updates, which marginalize over parameters of the clusters.

**Sampling the total number of latent events** Finally, we have at least two choices when it comes to updating the hyperparameters  $\alpha$ ,  $\beta$ , and the latent event intensity  $\bar{L}(\mathcal{X})$ . First, we can place a prior distribution over them and sample their conditional distribution. Conditional sampling is most easily accomplished by introducing the total number of latent events as an auxiliary variable (recall that the number of latent events was collapsed out in the derivation of the partition distribution). The following lemma gives the necessary conditional distribution.

**Lemma 2.** *In a Neyman-Scott process with gamma weights (Assumption 1), the number of empty clusters — i.e. the number of latent events that produce zero observed data points — is a Poisson random variable that is independent of the number of occupied clusters,*

$$L - |\mathcal{C}| \sim \text{Po}\left(\bar{L}(\mathcal{X}) \left(\frac{\beta}{1 + \beta}\right)^\alpha\right). \quad (23)$$

Interestingly, the mean of this conditional distribution is the same as the ratio in Lemma 1. The proof is in Appendix A.



**Sampling the latent event rate** Many Neyman-Scott processes, including the three examples above, parameterize the total measure of the latent event intensity as a linear function of the volume,  $\bar{L}(\mathcal{X}) = \bar{\nu}|\mathcal{X}|$ . Under a conjugate gamma prior  $\bar{\nu} \sim \text{Ga}(\alpha_\nu, \beta_\nu)$ , its conditional distribution is,

$$p(\bar{\nu} | L) = \text{Ga}(\bar{\nu} | \alpha_\nu + L, \beta_\nu + |\mathcal{X}|). \quad (24)$$

**Sampling the parameters of the weight distributions** Similarly, we can introduce auxiliary weights for the empty clusters from their gamma conditional distribution,

$$w_l \sim \text{Ga}(\alpha, \beta + 1) \quad \text{for } l = |\mathcal{C}| + 1, \dots, L \quad (25)$$

and then sample the hyperparameters  $\alpha$  and  $\beta$  from their conditional distribution,

$$p(\alpha, \beta | \{w_l\}_{l=1}^L) \propto p(\alpha, \beta) \prod_{l=1}^L \text{Ga}(w_l | \alpha, \beta). \quad (26)$$

If the prior factors as  $p(\alpha, \beta) = p(\alpha) \text{Ga}(\beta | \alpha_\beta, \beta_\beta)$ , the conditional distribution of the inverse scale is,

$$p(\beta | \{w_l\}_{l=1}^L) = \text{Ga}\left(\beta | \alpha_\beta + L\alpha, \beta_\beta + \sum_{l=1}^L w_l\right). \quad (27)$$

The shape parameter  $\alpha$  does not have a simple conjugate prior, but is amenable to Metropolis-Hastings updates. However, we prefer to treat  $\alpha$  as a hyperparameter and select it via cross-validation. Further details on hyperparameter selection, MCMC initialization, and approximate sampling via parallel MCMC are provided in Appendix C.

## 6 Experiments

We study the collapsed Gibbs algorithms for the Neyman-Scott process model on synthetic data as well as real neural recordings and document streams. All of the code for our experiments is written in the Julia programming language [Bezanson et al., 2017] and made publicly available in the Github repository `NeymanScottProcesses.jl`.<sup>2</sup> Across datasets, we find that the NSP offers a compelling alternative to existing clustering models in tasks like sequence detection in neural spike train data and event detection in document streams.

### 6.1 Synthetic data validation

In our first experiment, we compare the NSP with the DPMM on a synthetic dataset. We find that DPMM cannot model data from NSP well: it leads to inaccurate cluster assignments and a biased estimate of the number of clusters.

We generate synthetic data from a 2D Neyman-Scott process across the unit square  $\mathcal{X} = [0, 1]^2$  with gamma weights and Gaussian clusters, as described in Example 1 (see Figure 3, panel A). We set the background rate to zero for a fair comparison to the DPMM, which does not normally include such a

<sup>2</sup>Available at [github.com/lindermanlab/NeymanScottProcesses.jl](https://github.com/lindermanlab/NeymanScottProcesses.jl).

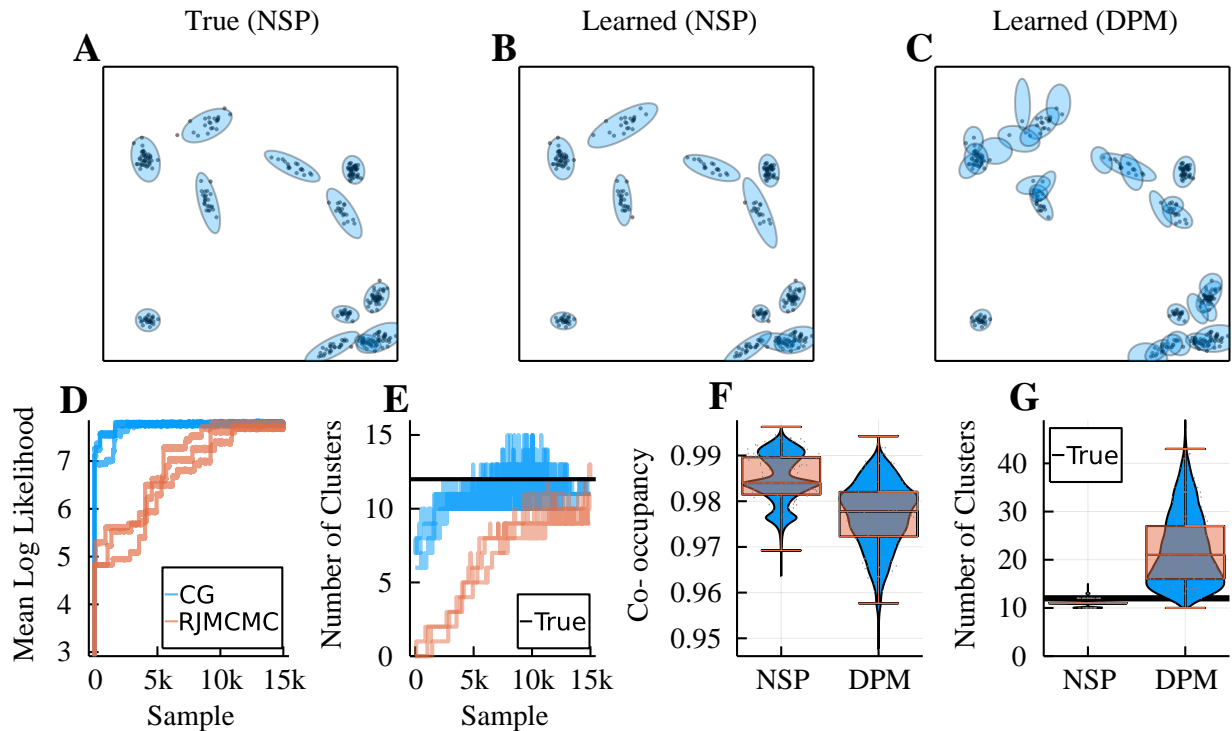


Figure 3: Performance of the Neyman-Scott process (NSP) and the Dirichlet process mixture model (DPMM) on synthetic 2D NSP data. **(A)** True data, generated by a Neyman-Scott process. Each observed event is colored according to its parent latent event. **(B)** Inferred parent assignments after inference with a Neyman-Scott process. **(C)** Same as (B), but using a DPMM. **(D-E)** Log-likelihood (D) and inferred number of clusters (E) of the data during Neyman-Scott process inference using collapsed Gibbs (CG) and reversible-jump MCMC with birth-death moves (RJMCMC). Inference consisted of 150 rounds of annealing, each for 100 samples. Each algorithm was run three times. **(F-G)** Distribution latent event assignment co-occupancy accuracy (F) and inferred number of clusters (G) for the NSP and DPM. Data from the last 5000 samples of all three chains is displayed. As expected, the DPM significantly overestimates the true number of clusters.

cluster. We then fit both an NSP and a DPMM to the generated data. Specifically, for each model, we run the proposed collapsed Gibbs sampling algorithm for 1000 samples and 3 independent chains. To accelerate mixing, we use a simple annealing procedure, fixing the mean of  $w_l$  and lowering the variance of  $\text{Ga}(w; \alpha, \beta)$  every 100 samples. The joint log-likelihood during inference is shown in Figure 3, Panel D.

Figure 3, panels B and C show the resulting parent assignments at the end of sampling one of the three chains, for each the NSP and the DPMM. We observe that the inferred assignments using the NSP qualitatively outperform those of the DPMM. To quantitatively assess the accuracy of the inferred parent assignments, we use *co-occupancy accuracy*. Let  $z$  and  $z'$  denote the parent assignments obtained from partitions  $\mathcal{C}$  and  $\mathcal{C}'$ , assuming arbitrary ordering of their clusters. The co-occupancy accuracy is defined as,

$$\text{accuracy}(z, z') = \frac{1}{N^2} \sum_{n=1}^N \sum_{m=1}^N \mathbb{I}[z_n = z_m] \mathbb{I}[z'_n = z'_m] + \mathbb{I}[z_n \neq z_m] \mathbb{I}[z'_n \neq z'_m],$$

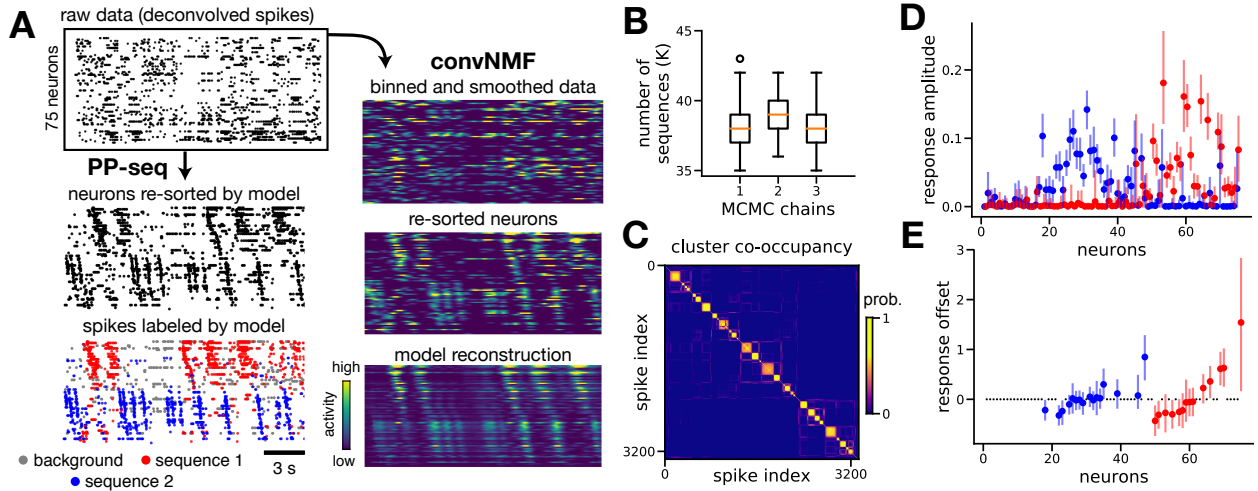


Figure 4: Zebra Finch HVC data. (A) Raw spike train (top) and sequences revealed by the Neyman-Scott process (left) and convNMF (right). (B) Box plots summarizing samples from the posterior on number of sequences,  $K$ , derived from three independent MCMC chains. (C) Co-occupancy matrix summarizing probabilities of spike pairs belonging to the same sequence. (D) Credible intervals for evoked amplitudes for sequence type 1 (red) and 2 (blue). (E) Credible intervals for response offsets (same order and coloring as D). Estimates are suppressed for small-amplitude responses (gray dots).

where  $\mathbb{I}[\cdot]$  is the binary indicator function. Panel F shows the co-occupancy accuracy of the resulting partition for the last 5000 samples of each chain. Finally, Panel G shows the inferred number of clusters over the same duration. The NSP infers both co-occupancy and the number of clusters more accurately than the DPMM. These results suggest that the DPMM is not an appropriate model for fitting data generated by an NSP (or an MFMM, see [Miller and Harrison \[2018\]](#) for additional examples).

## 6.2 Application: Detecting sequences in neural spike trains

We next apply the Neyman-Scott process model to perform sequence detection in neural data. With multielectrode arrays, neuroscientists can record the times at which individual neurons fire action potentials, or *spikes*. A collection of spike times from one or more neurons is called a *spike train*. In many experimental settings—including studies of working memory [[Goldman, 2009](#)], motor production [[Hahnloser et al., 2002](#)], and navigation [[Davidson et al., 2009](#)—groups of neurons (sometimes called “ensembles”) are hypothesized to fire repeatedly in sequences. Identifying these sequences in spike train data is a longstanding problem that has spurred a wide variety of modeling approaches [[Abeles and Gat, 2001](#), [Russo and Durstewitz, 2017](#), [Peter et al., 2017](#), [Quaglio et al., 2018](#), [Maboudi et al., 2018](#), [Mackevicius et al., 2019](#)]. The results shown below were previously presented as a conference paper, which contains additional detail for this application of Neyman-Scott process models [[Williams et al., 2020a](#)].

We model the spike train as a marked point process generated by the Neyman-Scott process presented in Example 2. The only difference is that we add a background intensity  $\lambda_0(x, y) = \bar{\lambda}_0 \text{Cat}(y | a_0)$ , where  $\bar{\lambda}_0$  determines the rate of background spikes across all neurons and  $a_0 \in \Delta_Y$  is a distribution over neurons.

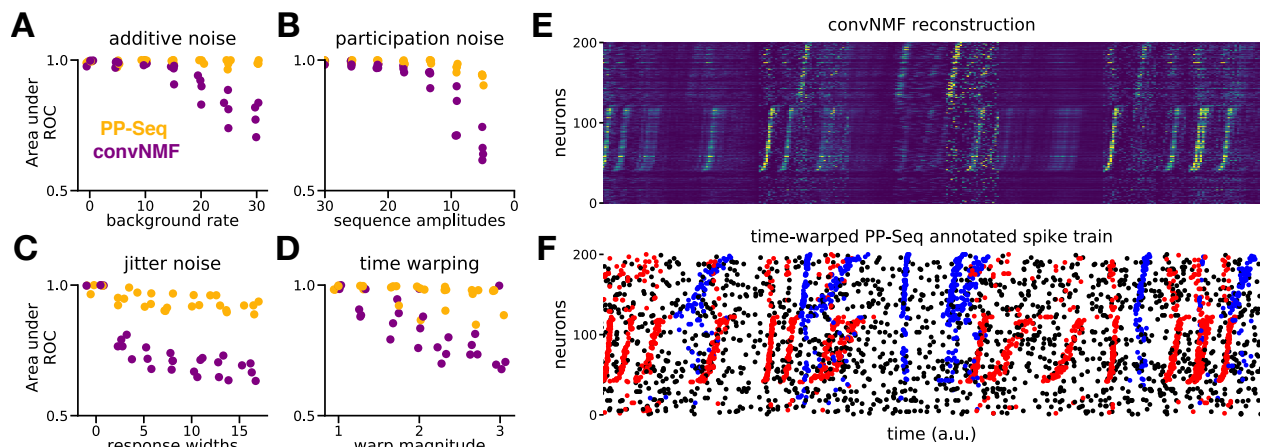


Figure 5: The Neyman-Scott process model for neural sequence detection is more robust to various forms of noise than convNMF. (A-D) Comparison of the Neyman-Scott process and convNMF to detect sequence times in synthetic data with varying amounts of noise. Panel D shows the performance of the time-warped variant of the Neyman-Scott process. (E) convNMF reconstruction of a spike train containing sequences with 9-fold time warping. (F) Performance of time-warped the Neyman-Scott process on the same data as panel E.

### 6.2.1 Zebra Finch Higher Vocal Center (HVC)

We applied the Neyman-Scott process to a recording of higher vocal center (HVC) premotor neurons in a zebra finch,<sup>3</sup> which generate sequences that are time-locked to syllables in the bird’s courtship song. Figure 4A shows a qualitative comparison of the performance of convNMF and the Neyman-Scott process for neural sequence detection. The raw data (top panel) showed no visible spike patterns; however, clear sequences were revealed by sorting the neurons lexicographically by preferred sequence type and the temporal offset parameter, as inferred by the Neyman-Scott process. While both models extracted similar sequences, the Neyman-Scott process provided a finer scale annotation of the final result, offering, for example, attributions at the level of individual spikes to sequences (bottom left of Figure 4A).

Further, the Neyman-Scott process offered uncertainty estimates for key parameters via the MCMC samples. Figure 4B summarizes uncertainty in the total number of sequence events, i.e.  $K = |\mathcal{C}|$ , pooled over three independent MCMC runs with different random seeds—all chains converged to similar estimates; the uncertainty is largely due to the rapid sequences (in blue) shown in panel A. Figure 4C displays a co-occupancy matrix where element  $(i, j)$  corresponds to the probability that spike  $i$  and spike  $j$  were attributed to the same sequence. Finally, Figure 4D-E shows the amplitude and offset for each neuron’s sequence-evoked response with 95% posterior credible intervals. These results naturally fall out of the probabilistic construction of the the Neyman-Scott process model, but have no obvious analogue in convNMF.

### 6.2.2 Time Warping Extension and Robustness to Noise

To compare the robustness of the Neyman-Scott process and convNMF under more challenging circumstances, we created a simple synthetic dataset with  $S = 1$  sequence type and  $N = 100$  neurons.

<sup>3</sup>These data are available at <http://github.com/FeeLab/seqNMF>; originally published in Mackevicius et al. [2019].

We varied four parameters to manipulate the difficulty of sequence extraction: the rate of background spikes,  $\bar{\lambda}_0$  (“additive noise,” Figure 5A), the expected number of spikes per sequence,  $w_l$  (“participation noise”, Figure 5B), the expected variance of the Gaussian impulse responses,  $\sigma_{y,s}$  (“jitter noise”, Figure 5C), and, finally, the maximal time warping coefficient (see Figure 5D). All simulated datasets involved sequences with low spike counts ( $\mathbb{E}[w_l] < 100$  spikes). In this regime, the Poisson likelihood criterion used by the Neyman-Scott process was better matched to the statistics of the spike train. Since convNMF optimizes an alternative loss function (squared error instead of Poisson likelihood) we compared the models by their ability to extract the ground truth sequence event times. Using area under receiver operating characteristic (ROC) curves as a performance metric, we saw favorable results for the Neyman-Scott process as noise levels were increased.

Experimental recordings show substantial variability in the duration of sequences [Davidson et al., 2009]. To account for this variability, we constructed a “time-warped” neural sequence detection model by augmenting the latent events in the Neyman-Scott process with an additional parameter. Now, we have  $\theta_l = (\theta_l^{(s)}, \theta_l^{(f)})$  where  $\theta_l^{(s)} \in \{1, \dots, S\}$  denotes the discrete type of the  $l$ -th latent event (a.k.a. sequence), and  $\theta_l^{(f)} \in \{1, \dots, F\}$  is an index into a discrete set of time-warping factors  $\{\tau_1, \dots, \tau_F\} \subset \mathbb{R}_+$ , which are symmetrically arranged around 1. If the time-warping factor is greater than 1, the sequence unfolds slower than average; if it is less than 1, the sequence unfolds faster than average. This time-warping property is captured by the following model,

$$p(x, y \mid m_l, \theta_l) = \text{Cat}(y \mid a_{\theta_l^{(s)}}) \cdot \mathcal{N}(x \mid m_l + \tau_{\theta_l^{(f)}} b_{y, \theta_l^{(s)}}, \tau_{\theta_l^{(f)}} \sigma_{y, \theta_l^{(s)}}^2). \quad (28)$$

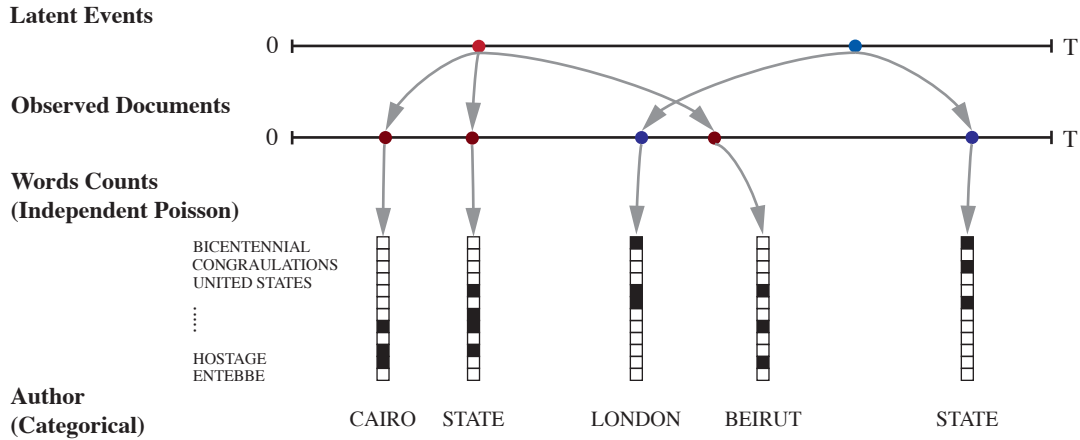
Under this model, faster sequences ( $\tau$ ’s) have shorter offsets and smaller variances. Importantly, the parameters of each latent event are discrete values  $\theta_l \in \{1, \dots, S\} \times \{1, \dots, F\}$ . As such, we can still perform the marginal likelihood calculations, integrating over  $\theta_l$  and  $m_l$ , analytically.

We demonstrated the abilities of the time-warped model further in Figure 5E-F. Here, we show a synthetic dataset containing sequences with 9-fold variability in their duration, which is similar to levels observed in some experimental systems Davidson et al. [2009]. While convNMF failed to reconstruct many of these warped sequences, the Neyman-Scott process model identified sequences that were closely matched to ground truth.

### 6.3 Application: Detecting world events in streams of diplomatic cables

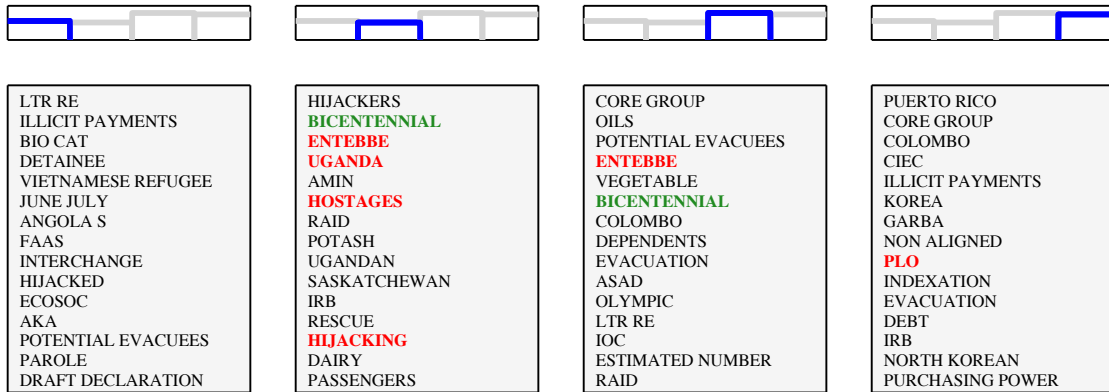
Detecting important events from historical documents is a common task for historians [Howell and Prevenier, 2001], and large-scale digital corpora offer new challenges and opportunities in this domain. Here we develop a Neyman-Scott process model to perform event detection in document streams. We study a dataset of US State Department declassified cables from the 1970s [Chaney et al., 2016], which spans a duration of  $T = 40$  days (June 21–July 31, 1976) and totals  $N = 34,732$  cables. The cables can be thought of as archaic text messages between diplomatic entities, or nodes. Each cable is associated with a time stamp,  $x_n \in [0, T]$ , and a mark,  $y_n = (y_n^{(a)}, y_n^{(c)})$ , where  $y_n^{(a)} \in \{1, \dots, A\}$  specifies the author and  $y_n^{(c)} \in \mathbb{N}_0^V$  is a vector of word counts for vocabulary of size  $V$ . Here, we have  $A = 2360$  authors and a  $V = 21,819$  word vocabulary.

To identify historical events with the cables dataset, we posit that: (1) each node sends out *background cables* about regional affairs, e.g. a Thailand entity regularly sends out cables about affairs in Southeast Asia; and (2) when a salient event occurs, some nodes will send out *event cables*.



**Baseline Model**

Average Predictive Log Likelihood: -196.9



**Neyman-Scott Process**

Average Predictive Log Likelihood: -189.1

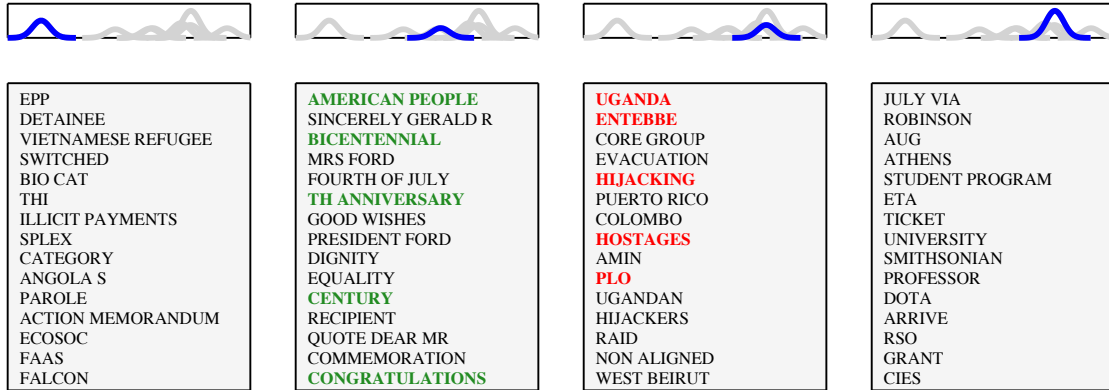


Figure 6: Document stream detection model. (top) Schematic of document stream model. A Neyman-Scott process generates events marked with a high-dimensional word count vector and a categorical label. (middle) Latent event amplitude and representative words produced by fitting embassy data with (discretized) baseline model. (bottom) Same as in the middle row, but using the Neyman-Scott process.

With this intuition, we model the cables with the Neyman-Scott process described in Example 3. The observed cables of all nodes are driven by latent “world events” with times, weights, and parameters that specify the distribution over authors and words. The only difference from the example model is that we add a background intensity,

$$\lambda_0(x, y) = \bar{\lambda}_0 \text{Cat}(y^{(a)} \mid \theta_0^{(a)}) \prod_{v=1}^V \text{Po}(y_v^{(c)} \mid \phi_{y^{(a)}, v}), \quad (29)$$

where  $\bar{\lambda}_0$  sets the rate of background cables,  $\theta_0^{(a)} \in \Delta_A$  is a distribution over background cable authors, and  $\phi_{a, v}$  specifies the rate of author  $a$  using word  $v$  in its background cables. The latter parameter is allowed to vary from one author to the next since different authors will use different terms in their day-to-day correspondence. Our goal is to infer the timestamps and word intensities of the latent events, as encoded in its parameters  $\theta_l$  (defined in Example 3), since these represent precisely the important world events we are after. Figure 6A shows a schematic that describes this data generating process.

We compared this Neyman-Scott process model for document streams to a baseline clustering model on this dataset similar to the model proposed by Chaney et al. [2016]. Both models allow for background cables with sender-specific rates and word distributions. The models differ in how they handle latent world events. Whereas the Neyman-Scott process models the cables data as a continuous-time process with latent events, the baseline model bins the time into one-week intervals and allows one latent event per week. Thus, the baseline model must necessarily combine contemporaneous world events into one cluster.

To compare the Neyman-Scott process model and the baseline model quantitatively, we compare the predictive log-likelihoods produced on held-out regions of the data. In particular, we hold out 10% of the event space by masking 10% of the observed time interval (4 randomly chosen days) for each embassy during inference. The baseline model achieves a predictive likelihood of  $-196.9$  nats/document whereas the NSP achieves  $-189.1$  nats/document, suggesting the NSP better generalizes to out-of-sample data.

Figure 6B-C presents the important diplomatic events detected by both models. The Neyman-Scott process model inferred two important and contemporaneous events: one about a celebration in the United States (green) and another about a hostage event involving Uganda (red), as seen in the top words shown in Figure 6. The first event points to United States Bicentennial, which celebrated the 200th anniversary of adopting the Declaration of Independence [Halloran, 1976]. The second event points to Operation Entebbe, which was a hostage-rescue mission in Uganda ordered by Israel Defence Forces [Smith, 1976].

Notably, the Neyman-Scott process model was able to distinguish temporally overlapping events. It inferred that the two important events detected were temporally overlapping. This inference was consistent with historical facts: both the bicentennial celebration and Operation Entebbe indeed occurred on the same day in history (July 4, 1976). In contrast, the baseline clustering model (Figure 6, middle) merged the bicentennial celebration event and Operation Entebbe since they both happened in the same week. This result illustrates the modeling power of Neyman-Scott processes for document streams: its continuous-time nature allows for the detection of overlapping latent events with both temporal- and sender-specificity.

## 7 Discussion

Neyman-Scott processes (NSPs) are doubly stochastic point processes that generated clusters of data points. Like Dirichlet process mixture models (DPMMs) and mixture of finite mixture models (MFMMs), the number of clusters is a random variable. NSPs, however, probabilistically model the number of observed within an observed spatiotemporal region, making them well suited to many applications in spatial statistics.

NSPs are not the only point processes that give rise to clusters of events. For example, Hawkes processes [Hawkes, 1971] produce clusters via a self-excitatory model: each event increases the probability of subsequent events. There has been a resurgence of interest in these models, and recent work has generalized the basic Hawkes process [Wang et al., 2012, Zhou et al., 2013, Linderman and Adams, 2014, Wu et al., 2019, Dutta et al., 2020], established new theory [Chen et al., 2017a], incorporated neural networks into the model [Mei and Eisner, 2016, Zuo et al., 2020, Zhang et al., 2020a], developed new inference and estimation algorithms [Simma and Jordan, 2010, Halpin, 2012, Rasmussen, 2013, Wheatley et al., 2016, Chen et al., 2017b, Shelton et al., 2018, Kirchner and Bercher, 2018, Zhang et al., 2020b], and specialized them to new domains like email and social media exchanges [Gomez-Rodriguez et al., 2010, Blundell et al., 2012, Farajtabar et al., 2015, Guo et al., 2015, He et al., 2015, Kobayashi and Lambiotte, 2016, Li et al., 2017, Mohler et al., 2018], online education [Jiang et al., 2021], crime modeling [Mohler et al., 2011], biology [Carstensen et al., 2010, Verma et al., 2021], healthcare [Bao et al., 2017], and epidemiology [Choi et al., 2015, Garetto et al., 2021, Chiang et al., 2021]. One advantage of Hawkes processes is that parameters can often be inferred by simple maximum likelihood estimation. However, Hawkes processes are rather unnatural models for purely spatial data where there is no obvious ordering of events, or where it is unnatural for one observed event to directly trigger another. It would be interesting to consider hybrid models that inherit some of the computational benefits of Hawkes processes while maintaining the latent variable formulation of NSPs.

Traditionally, parameter estimation and latent event inference in Neyman-Scott processes have been done via moment-matching or reversible jump MCMC methods. The former is limited in scope, requiring strong assumptions about the nature of the latent events and their impulse responses; the latter is quite general, but its performance is limited by our ability to craft efficient Metropolis-Hastings proposals. Here, we proposed a novel collapsed Gibbs sampling algorithm for Neyman-Scott processes with gamma weights (Assumption 1), an assumption that still permits a wide family of models, as showcased in our experiments.

We also showed how Neyman-Scott processes with gamma weights are intimately related to mixture of finite mixture models and Bayesian nonparametric mixture models derived from the Dirichlet process and the Pitman-Yor process. Specifically, the NSP with gamma weights converges to a Dirichlet process mixture model in a particular limit. In hindsight, this relationship is intuitive: the random measure induced by the latent events is an atomic distribution with gamma-distributed weights, and in the limit of infinitely many atoms with weights going to zero, we recover a gamma process. Indeed, the gamma process, once normalized, yields a Dirichlet process. In this sense, the NSP is very complementary to the two-parameter Pitman-Yor process. Both contain the Dirichlet process as a limiting case, but they approach this limit via different constructions.

One advantage of the Neyman-Scott process is that it is naturally extended to incorporate background events. The analogous extension in an MFMM or DPMM is to have an extra cluster that is always present



and has its own unique parameterization. While not implausible, this type of extension seems to be rare in practice. In our experiments, we found that the background cluster offered a useful way of separating data points due to latent events—the “signal” of interest—from the data points that were otherwise hard to explain—the “noise”. Without a background cluster, nonparametric mixture models have to create spurious clusters to explain those data points.

Our experiments highlighted the breadth of spatiotemporal clustering problems amenable to Neyman-Scott process models. In addition to the neural sequence detection models, which we presented in earlier work [Williams et al., 2020b], we also included synthetic data experiments to contrast NSPs with DPMMs and showed how the latter is prone to over-segmentation. Then we introduced a novel Neyman-Scott process formulation suited to detecting latent events underlying document streams and showed that it could detect contemporaneous latent events based on the types of vocabulary they elicited and the senders who discussed them. These are but two example applications, and it is easy to envision applications in other domains like ecology (e.g. modeling plant locations or rainfall distributions), epidemiology (e.g. modeling disease outbreaks), astronomy (e.g. modeling galaxy locations in survey data), seismology (e.g. modeling earthquake occurrences), and more.

Future work could aim to relax the key assumption of this paper—namely, that the latent events contain independent, gamma-distributed weights—with a model that allows for some dependency. Previous work on dependent Dirichlet processes may offer some ways of addressing this limitation [Müller and Rodriguez, 2013, Ch. 5]. Likewise, recent work on deep NSPs offers an alternative way of constructing rich point process models by stacking Neyman-Scott processes hierarchically [Hong and Shelton, 2021]. Ultimately, Neyman-Scott processes connect the world of doubly-stochastic point processes to Bayesian nonparametric mixture models, and we suspect there are many fruitful possibilities at this intersection.

## Acknowledgements

We thank David Blei and Peter Orbanz for many helpful discussions. We also thank Allison Chaney and Matthew Connelly for providing the preprocessed dataset of US State Department declassified cables. This work was supported by the U.S. Department of Energy, Office of Science, Office of Advanced Scientific Computing Research, Department of Energy Computational Science Graduate Fellowship under Award Number DE-SC0021110 to AD. This work was funded by grants to SWL from the NIH Brain Initiative (NINDS, U19NS113201 and R01NS113119) and the Simons Collaboration on the Global Brain (SCGB, 697092).

## A Proofs

*Proof of Theorem 1.* Our derivation follows the approach of Miller and Harrison [2018] for mixture of finite mixture models, but we adapt it to Neyman-Scott processes with gamma weights. The major difference is that the number of data points is a random variable in the NSP, so the distribution above is over partitions of random size. First, return to the generative process described in Algorithm 3 and integrate over the latent event amplitudes to obtain the marginal distribution on latent cluster sizes

given the total number of latent events  $L$ . We have,

$$\begin{aligned}
p(N_1, \dots, N_L | L) &= \prod_{l=1}^L \int \text{Po}(N_l | \gamma_l) \text{Ga}(\gamma_l | \alpha, \beta) d\gamma_l \\
&= \prod_{l=1}^L \text{NB}(N_l | \alpha, (1 + \beta)^{-1}) \\
&= \prod_{l=1}^L \frac{\Gamma(N_l + \alpha)}{N_l! \Gamma(\alpha)} \left( \frac{\beta}{1 + \beta} \right)^\alpha \left( \frac{1}{1 + \beta} \right)^{N_l} \\
&= \left( \frac{\beta}{1 + \beta} \right)^{L\alpha} \left( \frac{1}{1 + \beta} \right)^N \prod_{l=1}^L \frac{\Gamma(N_l + \alpha)}{N_l! \Gamma(\alpha)}.
\end{aligned}$$

Let  $z_n \in \{1, \dots, L\}$  denote the parent assignment of the  $n$ -th data point. There are  $\binom{N}{N_1, \dots, N_L}$  parent assignments consistent with the latent cluster sizes  $N_1, \dots, N_L$ , and they are all equally likely under the prior, so the conditional probability of the parent assignments is,

$$\begin{aligned}
p(\{z_n\}_{n=1}^N | L) &= \binom{N}{N_1, \dots, N_L}^{-1} \left( \frac{\beta}{1 + \beta} \right)^{L\alpha} \left( \frac{1}{1 + \beta} \right)^N \prod_{l=1}^L \frac{\Gamma(N_l + \alpha)}{N_l! \Gamma(\alpha)} \\
&= \frac{1}{N!} \left( \frac{\beta}{1 + \beta} \right)^{L\alpha} \left( \frac{1}{1 + \beta} \right)^N \prod_{l=1}^L \frac{\Gamma(N_l + \alpha)}{\Gamma(\alpha)}
\end{aligned}$$

The parent assignments above induce a partition, but technically they assume an ordering of the latent events. Moreover, if some of the latent events fail to produce any observed events, they will not be included in the partition. In performing a change of variables from parent assignments  $\{z_n\}_{n=1}^N$  to partitions  $\mathcal{C}$ , we need to sum over latent event assignments that produce the same partition. There are  $\binom{L}{|\mathcal{C}|} |\mathcal{C}|! = \frac{L!}{(L-|\mathcal{C}|)!}$  such assignments if there are  $L$  latent events but only  $|\mathcal{C}|$  parts in the partitions. Thus,

$$p(N, \mathcal{C} | L) = \frac{L!}{(L - |\mathcal{C}|)!} \frac{1}{N!} \left( \frac{\beta}{1 + \beta} \right)^{L\alpha} \left( \frac{1}{1 + \beta} \right)^N \prod_{\mathcal{C}_k \in \mathcal{C}} \frac{\Gamma(|\mathcal{C}_k| + \alpha)}{\Gamma(\alpha)}.$$

Clearly,  $L$  must be at least  $|\mathcal{C}|$  in order to produce the partition.

Finally, we sum over the number of latent events  $L$  to obtain the marginal probability of the partition,

$$\begin{aligned}
p(N, \mathcal{C}) &= \sum_{L=|\mathcal{C}|}^{\infty} \text{Po}(L | \bar{L}(\mathcal{X})) p(N, \mathcal{C} | L) \\
&= V_{N, |\mathcal{C}|} \prod_{\mathcal{C}_k \in \mathcal{C}} \frac{\Gamma(|\mathcal{C}_k| + \alpha)}{\Gamma(\alpha)},
\end{aligned}$$

where

$$V_{N, |\mathcal{C}|} = \frac{1}{N!} \left( \frac{1}{1 + \beta} \right)^N \sum_{L=|\mathcal{C}|}^{\infty} \text{Po}(L | \bar{L}(\mathcal{X})) \frac{L!}{(L - |\mathcal{C}|)!} \left( \frac{\beta}{1 + \beta} \right)^{L\alpha}. \quad (30)$$

□

*Proof of Theorem 2.* Let  $\mathcal{C}$  be a partition of  $\{1, \dots, N\}$  and  $\mathcal{C} \setminus N$  denote the partition of  $\{1, \dots, N-1\}$  obtained after removing  $N$  from  $\mathcal{C}$ . The transition operator defined in the theorem guarantees that  $\mathcal{C}' = \mathcal{C} \setminus N$ . We will proceed by induction. Suppose  $\mathcal{C}'$  is distributed as  $p(\mathcal{C}' \mid N-1)$ . The marginal distribution of the partition  $\mathcal{C}$  obtained by the transition operator is,

$$q(\mathcal{C}) = \sum_{\mathcal{C}'} p(\mathcal{C}' \mid N-1) p(\mathcal{C} \mid \mathcal{C}') \quad (31)$$

$$= \frac{V_{N-1, |\mathcal{C} \setminus N|}}{p(N-1)} \prod_{\mathcal{C}_k \in \mathcal{C} \setminus N} \left[ \frac{\Gamma(|\mathcal{C}_k| + \alpha)}{\Gamma(\alpha)} \right] p(\mathcal{C} \mid \mathcal{C} \setminus N). \quad (32)$$

There are two cases to consider. First, suppose  $N$  was added to an existing cluster (i.e.  $\mathcal{C}_k \in \mathcal{C} \setminus N$  and  $\mathcal{C}_k \cup \{N\} \in \mathcal{C}$ ). Then,

$$q(\mathcal{C}) \propto \frac{V_{N-1, |\mathcal{C} \setminus N|}}{p(N-1)} \prod_{\mathcal{C}_k \in \mathcal{C} \setminus N} \left[ \frac{\Gamma(|\mathcal{C}_k| + \alpha)}{\Gamma(\alpha)} \right] (|\mathcal{C}_k| + \alpha) \quad (33)$$

$$\propto \frac{V_{N-1, |\mathcal{C} \setminus N|}}{p(N-1)} \prod_{\mathcal{C}_k \in \mathcal{C}} \frac{\Gamma(|\mathcal{C}_k| + \alpha)}{\Gamma(\alpha)} \quad (34)$$

Second, suppose that a new cluster was created (i.e.  $\{N\} \in \mathcal{C}$ ). Then,

$$q(\mathcal{C}) \propto \frac{V_{N-1, |\mathcal{C} \setminus N|}}{p(N-1)} \prod_{\mathcal{C}_k \in \mathcal{C} \setminus N} \left[ \frac{\Gamma(|\mathcal{C}_k| + \alpha)}{\Gamma(\alpha)} \right] \left( \alpha \frac{V_{N, |\mathcal{C} \setminus N| + 1}}{V_{N, |\mathcal{C} \setminus N|}} \right) \quad (35)$$

$$\propto \frac{V_{N-1, |\mathcal{C} \setminus N|}}{p(N-1)} \frac{V_{N, |\mathcal{C}|}}{V_{N, |\mathcal{C} \setminus N|}} \prod_{\mathcal{C}_k \in \mathcal{C}} \frac{\Gamma(|\mathcal{C}_k| + \alpha)}{\Gamma(\alpha)} \quad (36)$$

Multiplying equations (34) and (36) by  $\frac{V_{N, |\mathcal{C} \setminus N|} p(N-1)}{V_{N-1, |\mathcal{C} \setminus N|}}$  and noting that  $|\mathcal{C} \setminus N| = |\mathcal{C}|$  when  $N$  is added to an existing cluster, the probability in both cases reduces to

$$q(\mathcal{C}) \propto V_{N, |\mathcal{C}|} \prod_{\mathcal{C}_k \in \mathcal{C}} \frac{\Gamma(|\mathcal{C}_k| + \alpha)}{\Gamma(\alpha)} \quad (37)$$

in both cases. Since this distribution is proportional to eq. (12) and  $\mathcal{C}$  is a partition of  $\{1, \dots, N\}$ , the normalizing constant must be  $p(N)$ . Thus,  $q(\mathcal{C}) = p(\mathcal{C} \mid N)$ .

To complete the proof, let's double check that the base case  $\mathcal{C} = \{\{1\}\}$  is indeed distributed

as  $p(\mathcal{C} \mid N = 1)$ ,

$$p(\mathcal{C} = \{\{1\}\} \mid N = 1) = \frac{V_{1,1}}{p(N = 1)} \cdot \frac{\Gamma(1 + \alpha)}{\Gamma(\alpha)} \quad (38)$$

$$= \frac{(1 + \beta)^{-1} \sum_{L=1}^{\infty} \text{Po}(L \mid \bar{L}(\mathcal{X})) \frac{L!}{(L-1)!} \left(\frac{\beta}{1+\beta}\right)^{L\alpha}}{\sum_{L=0}^{\infty} \text{Po}(L \mid \bar{L}(\mathcal{X})) \text{NB}(1 \mid L\alpha, (1 + \beta)^{-1})} \cdot \alpha \quad (39)$$

$$= \frac{(1 + \beta)^{-1} \sum_{L=1}^{\infty} \text{Po}(L \mid \bar{L}(\mathcal{X})) \frac{L!}{(L-1)!} \left(\frac{\beta}{1+\beta}\right)^{L\alpha}}{\sum_{L=0}^{\infty} \text{Po}(L \mid \bar{L}(\mathcal{X})) \frac{\Gamma(L\alpha+1)}{\Gamma(L\alpha)} (1 + \beta)^{-1} \left(\frac{\beta}{1+\beta}\right)^{L\alpha} \mathbb{I}[L > 0]} \cdot \alpha \quad (40)$$

$$= \frac{(1 + \beta)^{-1} \sum_{L=1}^{\infty} \text{Po}(L \mid \bar{L}(\mathcal{X})) L \left(\frac{\beta}{1+\beta}\right)^{L\alpha}}{(1 + \beta)^{-1} \sum_{L=1}^{\infty} \text{Po}(L \mid \bar{L}(\mathcal{X})) L\alpha \left(\frac{\beta}{1+\beta}\right)^{L\alpha}} \cdot \alpha \quad (41)$$

$$= 1. \quad (42)$$

This tedious algebra confirms the obvious fact that there is only one partition of the set  $\{1\}$ , so the base case is trivially distributed as  $p(\mathcal{C} \mid N)$ . The induction is complete.  $\square$

*Proof of Lemma 1.* Substituting the definition (30) and expanding the Poisson probability mass function,

$$\frac{V_{N,|\mathcal{C}|+1}}{V_{N,|\mathcal{C}|}} = \frac{\sum_{L=|\mathcal{C}|+1}^{\infty} \frac{1}{L!} e^{-\bar{\eta}|\mathcal{X}|} (\bar{\eta}|\mathcal{X}|)^L \frac{L!}{(L-|\mathcal{C}|-1)!} \left(\frac{\beta}{1+\beta}\right)^{L\alpha}}{\sum_{L=|\mathcal{C}|}^{\infty} \frac{1}{L!} e^{-\bar{\eta}|\mathcal{X}|} (\bar{\eta}|\mathcal{X}|)^L \frac{L!}{(L-|\mathcal{C}|)!} \left(\frac{\beta}{1+\beta}\right)^{L\alpha}} \quad (43)$$

$$= \frac{\sum_{L=|\mathcal{C}|}^{\infty} (\bar{\eta}|\mathcal{X}|)^{L+1} \frac{1}{(L-|\mathcal{C}|)!} \left(\frac{\beta}{1+\beta}\right)^{(L+1)\alpha}}{\sum_{L=|\mathcal{C}|}^{\infty} (\bar{\eta}|\mathcal{X}|)^L \frac{1}{(L-|\mathcal{C}|)!} \left(\frac{\beta}{1+\beta}\right)^{L\alpha}} \quad (44)$$

$$= \bar{\eta}|\mathcal{X}| \left(\frac{\beta}{1+\beta}\right)^{\alpha}. \quad (45)$$

$\square$

*Proof of Theorem 4.* The partition distribution changes slightly when we incorporate background data points. Intuitively, the background intensity is like a latent event that is always present. Let  $N_0$  denote the number of data points attributed to the background and let  $w_0(\mathcal{X}) = \int_{\mathcal{X}} \lambda_0(x) dx$  denote the integrated background intensity.

$$p(N_0, N_1, \dots, N_L \mid L) = \text{Po}(N_0 \mid w_0(\mathcal{X})) \prod_{l=1}^L \int \text{Po}(N_l \mid \gamma_l) \text{Ga}(\gamma_l \mid \alpha, \beta) d\gamma_l \quad (46)$$

$$= \text{Po}(N_0 \mid w_0(\mathcal{X})) \left(\frac{\beta}{1+\beta}\right)^{L\alpha} \left(\frac{1}{1+\beta}\right)^{N-N_0} \prod_{l=1}^L \frac{\Gamma(N_l + \alpha)}{N_l! \Gamma(\alpha)}. \quad (47)$$

There are  $\binom{N}{N_0, \dots, N_L}$  parent assignments consistent with the latent cluster sizes  $N_0, \dots, N_L$ , and they are all equally likely under the prior, so the conditional probability of the parent assignments is,

$$p(\{z_n\}_{n=1}^N | L) = \binom{N}{N_0, \dots, N_L}^{-1} \text{Po}(N_0 | w_0(\mathcal{X})) \left(\frac{\beta}{1+\beta}\right)^{L\alpha} \left(\frac{1}{1+\beta}\right)^N \prod_{l=1}^L \frac{\Gamma(N_l + \alpha)}{N_l! \Gamma(\alpha)} \quad (48)$$

$$= \frac{1}{N!} e^{-w_0(\mathcal{X})} w_0(\mathcal{X})^{N_0} \left(\frac{\beta}{1+\beta}\right)^{L\alpha} \left(\frac{1}{1+\beta}\right)^{N-N_0} \prod_{l=1}^L \frac{\Gamma(N_l + \alpha)}{\Gamma(\alpha)} \quad (49)$$

The parent assignments induce a partition, but technically they assume an ordering of the latent events. Moreover, if some of the latent events fail to produce any observed events, they will not be included in the partition. In performing a change of variables from parent assignments  $\{z_n\}_{n=1}^N$  to partitions  $\mathcal{C}$ , we need to sum over latent event assignments that produce the same partition. There are  $\binom{L}{|\mathcal{C}|} |\mathcal{C}|! = \frac{L!}{(L-|\mathcal{C}|)!}$  such assignments if there are  $L$  latent events but only  $|\mathcal{C}|$  parts in the partitions. Thus,

$$p(N, \mathcal{C}_0, \mathcal{C} | L) = \frac{L!}{(L-|\mathcal{C}|)! N!} e^{-w_0(\mathcal{X})} w_0(\mathcal{X})^{|\mathcal{C}_0|} \left(\frac{\beta}{1+\beta}\right)^{L\alpha} \left(\frac{1}{1+\beta}\right)^{N-|\mathcal{C}_0|} \prod_{\mathcal{C}_k \in \mathcal{C}} \frac{\Gamma(|\mathcal{C}_k| + \alpha)}{\Gamma(\alpha)}. \quad (50)$$

Of course,  $L$  must be at least  $|\mathcal{C}|$  in order to produce the partition. Summing over the number of latent events  $L$  yields the marginal probability of the partition,

$$p(N, \mathcal{C}_0, \mathcal{C}) = \sum_{L=|\mathcal{C}|}^{\infty} \text{Po}(L | \bar{L}(\mathcal{X})) p(N, \mathcal{C}_0, \mathcal{C} | L) \quad (51)$$

$$= \left(\frac{(N-|\mathcal{C}_0|)!}{N!}\right) e^{-w_0(\mathcal{X})} w_0(\mathcal{X})^{|\mathcal{C}_0|} (\mathcal{X})^{|\mathcal{C}_0|} V_{N-|\mathcal{C}_0|, |\mathcal{C}|} \prod_{\mathcal{C}_k \in \mathcal{C}} \frac{\Gamma(|\mathcal{C}_k| + \alpha)}{\Gamma(\alpha)}, \quad (52)$$

where  $V_{N-|\mathcal{C}_0|, |\mathcal{C}|}$  is defined by eq. (30) above.  $\square$

## B Random measure perspective on Neyman-Scott processes

Let

$$G(\mathcal{A}) = \sum_{l=1}^L w_l \delta_{(m_l, \theta_l)}(\mathcal{A}) \quad (53)$$

denote the random discrete measure on  $\mathcal{X} \times \Theta$  induced by a random sample of latent events from their Poisson process prior. (Here,  $\delta_{(m, \theta)}(\mathcal{A})$  is an indicator function that evaluates to 1 if  $(m, \theta) \in \mathcal{A}$  and 0 otherwise.) Under Assumption 1, the induced intensity is a homogenous Poisson random measure [Orbanz, 2014]. The mass in eq. (53) is the sum of functions applied to each point in a Poisson process, and as such it is a random variable. By Campbell's Theorem [Kingman, 1992, Ch. 3.2], its moment generating function is,

$$\mathbb{E}[e^{-tG(\mathcal{A})}] = \exp \left\{ \int_{\mathcal{X}} \int_{\mathbb{R}_+} \int_{\Theta} \nu(m, w, \theta) (e^{-tw \delta_{(m, \theta)}(\mathcal{A})} - 1) dm dw d\theta \right\} \quad (54)$$

$$= \exp \left\{ \bar{L}(\mathcal{X}) G_0(\mathcal{A}) \int_{\mathbb{R}_+} \text{Ga}(w | \alpha, \beta) (e^{-tw} - 1) dw \right\}, \quad (55)$$

where

$$G_0(\mathcal{A}) = \int_{\mathcal{X}} \int_{\Theta} p(m, \theta) \delta_{(m, \theta)}(\mathcal{A}) dm d\theta \quad (56)$$

is the marginal probability of the set  $\mathcal{A}$ . This will be the base measure of the Dirichlet process in the limit described in Corollary 3. Taking that limit, we have,

$$\lim_{\substack{\alpha \rightarrow 0 \\ \alpha \bar{L}(\mathcal{X}) \rightarrow \gamma}} \mathbb{E}[e^{-tG(\mathcal{A})}] = \lim_{\substack{\alpha \rightarrow 0 \\ \alpha \bar{L}(\mathcal{X}) \rightarrow \gamma}} \exp \left\{ \bar{L}(\mathcal{X}) G_0(\mathcal{A}) \int_{\mathbb{R}_+} \frac{\alpha \beta^\alpha}{\alpha \Gamma(\alpha)} w^{\alpha-1} e^{-\beta w} (e^{-tw} - 1) dw \right\} \quad (57)$$

$$= \exp \left\{ \gamma G_0(\mathcal{A}) \int_{\mathbb{R}_+} w^{-1} e^{-\beta w} (e^{-tw} - 1) dw \right\} \quad (58)$$

$$= \left( 1 + \frac{t}{\beta} \right)^{-\gamma G_0(\mathcal{A})}, \quad (59)$$

which follows from the fact that  $\Gamma(\alpha+1) = \alpha\Gamma(\alpha)$  and  $\Gamma(1) = 1$ , and from the Lévy-Khinchine representation of the gamma distribution. Eq. (59) is the MGF of a gamma distribution,  $G(\mathcal{A}) \sim \text{Ga}(\gamma G_0(\mathcal{A}), \beta)$ , so in this limit the random measure is a gamma process. Intuitively, the Neyman-Scott process with gamma weights approaches a gamma process in the limit where there are infinitely many latent events with weights going to zero. When the gamma process is normalized by its total mass it yields a Dirichlet process.

## C Inference Details

### C.1 Annealing

The intensity of weights  $\gamma_\ell$  is proportional to the gamma density  $\text{Ga}(\gamma_\ell | \alpha, \beta)$ , and these hyperparameters affect the mixing time of the Gibbs sampler. Intuitively, if there is little probability of low-weight latent events, the sampler is unlikely to create new latent events and is therefore slow to explore different partitions of observed events. This problem is common to other nonparametric Bayesian mixture models as well [Miller and Harrison, 2018, e.g.]. If, on the other hand, the variance of  $\text{Ga}(\alpha, \beta)$  is large relative to the mean, then the probability of forming new clusters is non-negligible and the sampler tends to mix more effectively. Unfortunately, this latter regime is also probably of lesser scientific interest, since the interesting latent events are typically large in amplitude. For example, in neuroscience settings, sequences of interest may involve many thousands of observed events, each potentially contributing a small number of spikes Buzsáki and Tingley [2018], Hahnloser et al. [2002].

To address this issue, we propose an annealing procedure to initialize the Markov chain. We fix the mean of  $\gamma_\ell$  and adjust  $\alpha$  and  $\beta$  to slowly lower variance of amplitude distribution. Initially, the sampler produces many small clusters of spikes, and as we lower the variance of  $\text{Ga}(\alpha, \beta)$  to a target value, the Markov chain typically combines these clusters into larger sequences. Finally, though we have not found it necessary, one could use alternative methods, like convolutional matrix factorization [Smaragdis, 2006, Degleris et al., 2019] to initialize the MCMC algorithm.

## C.2 Parallel MCMC

Resampling the partition (i.e. cluster assignments) is the primary computational bottleneck for the Gibbs sampler. For many datasets, we can improve performance substantially, at the cost of minor approximation error, by parallelizing the computation [Angelino et al. \[2016\]](#). Consider a set of observed events on the time interval  $[0, T]$ . Given  $P$  processors, we divide the dataset into intervals lasting  $T/P$  seconds, and allocate one interval per processor. The current global parameters,  $\Theta$ , are first broadcast to all processors. In parallel, the processors update the cluster assignments for the observed events in their interval, and then send back sufficient statistics describing each inferred cluster within their interval. After these sufficient statistics are collected on a single processor, the global parameters are re-sampled and then broadcast back to the processors to initiate another iteration. This algorithm introduces some error since clusters are not shared across processors. In essence, this introduces erroneous edge effects if a cluster is split across two processors. However, these errors are negligible when the cluster duration is much less than  $T/P$ , which we expect is the practical regime of interest.

## C.3 Cross-validation

We evaluate model performance by computing the log-likelihood assigned to held-out data. Partitioning the data into training and testing sets must be done somewhat carefully. For example, in the neural sequence detection example, we cannot withhold time intervals completely or else the model will not accurately predict latent sequences occurring in these intervals; likewise, we cannot withhold individual neurons completely or else the model will not accurately predict the response parameters of those held out cells. Thus, we adopt a “speckled” holdout strategy [Wold \[1978\]](#). We treat held-out spikes as missing data and sample them as part of the MCMC algorithm. (Their conditional distribution is fully specified by the generative model.) A similar approach holds for the diplomatic cables example, where we must ensure that we see at least one cable for each entity in order to estimate that entity’s parameters can be inferred. More generally, in spatial or spatiotemporal settings, we hold out random regions of space, as described in the main text.

## References

- M. Abeles and I. Gat. Detecting precise firing sequences in experimental data. *J. Neurosci. Methods*, 107 (1-2):141–154, May 2001.
- R. P. Adams, I. Murray, and D. J. C. MacKay. Tractable nonparametric Bayesian inference in Poisson processes with Gaussian process intensities. In *Proceedings of the 26th Annual International Conference on Machine Learning - ICML '09*, New York, New York, USA, 2009. ACM Press.
- E. Angelino, M. J. Johnson, and R. P. Adams. Patterns of scalable Bayesian inference. *Foundations and Trends® in Machine Learning*, 9(2-3):119–247, 2016.
- C. E. Antoniak. Mixtures of Dirichlet processes with applications to Bayesian nonparametric problems. *The Annals of Statistics*, pages 1152–1174, 1974.
- A. Baddeley, E. Rubak, and R. Turner. *Spatial Point Patterns: Methodology and Applications with R*. CRC Press, Nov. 2015.

- Y. Bao, Z. Kuang, P. Peissig, D. Page, and R. Willett. Hawkes process modeling of adverse drug reactions with longitudinal observational data. In *Machine learning for healthcare conference*, pages 177–190. PMLR, 2017.
- M. S. Bartlett. The spectral analysis of point processes. *J. R. Stat. Soc. Series B Stat. Methodol.*, 25(2): 264–296, 1963.
- J. Bezanson, A. Edelman, S. Karpinski, and V. B. Shah. Julia: A fresh approach to numerical computing. *SIAM Review*, 59(1):65–98, 2017. doi: 10.1137/141000671. URL <https://epubs.siam.org/doi/10.1137/141000671>.
- D. Blackwell and J. B. MacQueen. Ferguson distributions via Pólya urn schemes. *Ann. Stat.*, 1(2): 353–355, 1973.
- D. M. Blei and M. I. Jordan. Variational inference for Dirichlet process mixtures. *Bayesian Anal.*, 1(1): 121–143, Mar. 2006.
- C. Blundell, J. Beck, and K. A. Heller. Modelling reciprocating relationships with Hawkes processes. In *Advances in Neural Information Processing Systems*, pages 2600–2608, 2012.
- A. Brix. Generalized gamma measures and shot-noise Cox processes. *Adv. Appl. Probab.*, 31(4):929–953, 1999.
- G. Buzsáki and D. Tingley. Space and time: the hippocampus as a sequence generator. *Trends Cogn. Sci.*, 22(10):853–869, Oct. 2018.
- L. Carstensen, A. Sandelin, O. Winther, and N. R. Hansen. Multivariate Hawkes process models of the occurrence of regulatory elements. *BMC bioinformatics*, 11(1):1–19, 2010.
- A. J. Chaney, H. Wallach, M. Connelly, and D. M. Blei. Detecting and characterizing events. In *Proceedings of the 2016 Conference on Empirical Methods in Natural Language Processing*, EMNLP ’16, pages 1142–1152, 2016.
- S. Chen, A. Shojaie, E. Shea-Brown, and D. Witten. The multivariate Hawkes process in high dimensions: Beyond mutual excitation. *arXiv preprint arXiv:1707.04928*, 2017a.
- S. Chen, D. Witten, and A. Shojaie. Nearly assumptionless screening for the mutually-exciting multivariate Hawkes process. *Electronic journal of statistics*, 11(1):1207, 2017b.
- W.-H. Chiang, X. Liu, and G. Mohler. Hawkes process modeling of COVID-19 with mobility leading indicators and spatial covariates. *International journal of forecasting*, 2021.
- E. Choi, N. Du, R. Chen, L. Song, and J. Sun. Constructing disease network and temporal progression model via context-sensitive Hawkes process. In *2015 IEEE International Conference on Data Mining*, pages 721–726. IEEE, 2015.
- D. R. Cox. Some statistical methods connected with series of events. *J. R. Stat. Soc. Series B Stat. Methodol.*, 17(2):129–164, 1955.
- N. A. C. Cressie. *Statistics for spatial data*. Wiley, New York, 1993.
- D. J. Daley and D. Vere-Jones. *An Introduction to the Theory of Point Processes: Volume I: Elementary Theory and Methods*. Springer, New York, NY, 2003.



- T. J. Davidson, F. Kloosterman, and M. A. Wilson. Hippocampal replay of extended experience. *Neuron*, 63(4):497–507, Aug. 2009.
- A. Degleris, B. Antin, S. Ganguli, and A. H. Williams. Fast convolutive nonnegative matrix factorization through coordinate and block coordinate updates. *arXiv preprint arXiv:1907.00139*, 2019.
- P. J. Diggle. *Statistical Analysis of Spatial and Spatio-Temporal Point Patterns, Third Edition*. CRC Press, July 2013.
- H. S. Dutta, V. R. Dutta, A. Adhikary, and T. Chakraborty. HawkesEye: Detecting fake retweeters using Hawkes process and topic modeling. *IEEE Transactions on Information Forensics and Security*, 15: 2667–2678, 2020.
- M. D. Escobar and M. West. Bayesian density estimation and inference using mixtures. *J. Am. Stat. Assoc.*, 90(430):577–588, June 1995.
- M. Farajtabar, Y. Wang, M. Gomez Rodriguez, S. Li, H. Zha, and L. Song. COEVOLVE: A joint point process model for information diffusion and network co-evolution. In C. Cortes, N. D. Lawrence, D. D. Lee, M. Sugiyama, and R. Garnett, editors, *Advances in Neural Information Processing Systems 28*, pages 1954–1962. Curran Associates, Inc., 2015.
- M. Garetto, E. Leonardi, and G. L. Torrisi. A time-modulated Hawkes process to model the spread of COVID-19 and the impact of countermeasures. *Annual Reviews in Control*, 2021.
- A. Gnedin and J. Pitman. Exchangeable Gibbs partitions and Stirling triangles. *J. Math. Sci.*, 138(3): 5674–5685, Oct. 2006.
- M. S. Goldman. Memory without feedback in a neural network. *Neuron*, 61(4):621–634, Feb. 2009.
- M. Gomez-Rodriguez, J. Leskovec, and A. Krause. Inferring networks of diffusion and influence. *Proceedings of the ACM SIGKDD International Conference on Knowledge Discovery and Data Mining*, pages 1019–1028, 2010.
- P. J. Green. Trans-dimensional Markov chain Monte Carlo. *Oxford Statistical Science Series*, pages 179–198, 2003.
- F. Guo, C. Blundell, H. Wallach, and K. Heller. The Bayesian echo chamber: Modeling social influence via linguistic accommodation. In *Artificial Intelligence and Statistics*, pages 315–323, 2015.
- R. H. R. Hahnloser, A. A. Kozhevnikov, and M. S. Fee. An ultra-sparse code underlies the generation of neural sequences in a songbird. *Nature*, 419(6902):65–70, Sept. 2002.
- R. Halloran. 500,000 view capital’s bicentennial parade. *The New York Times*, Jul 1976.
- P. F. Halpin. An EM algorithm for Hawkes process. *Psychometrika*, 2, 2012.
- A. G. Hawkes. Spectra of some self-exciting and mutually exciting point processes. *Biometrika*, 58(1): 83–90, 1971.
- X. He, T. Rekatsinas, J. Foulds, L. Getoor, and Y. Liu. Hawkestopic: A joint model for network inference and topic modeling from text-based cascades. In *International Conference on Machine Learning*, pages 871–880, 2015.

- C. Hong and C. R. Shelton. Deep Neyman-Scott processes. *arXiv preprint arXiv:2111.03949*, 2021.
- M. C. Howell and W. Prevenier. *From reliable sources: An introduction to historical methods*. Cornell University Press, 2001.
- S. Jain and R. M. Neal. A split-merge Markov chain Monte Carlo procedure for the Dirichlet process mixture model. *J. Comput. Graph. Stat.*, 13(1):158–182, Mar. 2004.
- S. Jain and R. M. Neal. Splitting and merging components of a nonconjugate Dirichlet process mixture model. *Bayesian Anal.*, 2(3):445–472, Sept. 2007.
- L. Jiang, P. Wang, K. Cheng, K. Liu, M. Yin, B. Jin, and Y. Fu. EduHawkes: A Neural Hawkes Process Approach for Online Study Behavior Modeling. In *Proceedings of the 2021 SIAM International Conference on Data Mining (SDM)*, pages 567–575. SIAM, 2021.
- N. L. Johnson, A. W. Kemp, and S. Kotz. *Univariate discrete distributions*, volume 444. John Wiley & Sons, 2005.
- J. Kingman. *Poisson Processes*. Oxford Studies in Probability. Clarendon Press, 1992. ISBN 9780191591242.
- M. Kirchner and A. Bercher. A nonparametric estimation procedure for the Hawkes process: comparison with maximum likelihood estimation. *Journal of Statistical Computation and Simulation*, 88(6):1106–1116, 2018.
- R. Kobayashi and R. Lambiotte. TIDEH: Time-dependent Hawkes process for predicting retweet dynamics. In *Tenth International AAAI Conference on Web and Social Media*, 2016.
- S. Li, X. Gao, W. Bao, and G. Chen. FM-Hawkes: A Hawkes process based approach for modeling online activity correlations. In *Proceedings of the 2017 ACM on Conference on Information and Knowledge Management*, pages 1119–1128, 2017.
- S. Linderman and R. Adams. Discovering latent network structure in point process data. In *International Conference on Machine Learning*, pages 1413–1421. PMLR, 2014.
- A. Y. Lo. On a class of Bayesian nonparametric estimates: I. Density estimates. *Annals of Statistics*, 12(1):351–357, Mar. 1984.
- E. Lukacs. A characterization of the gamma distribution. *The Annals of Mathematical Statistics*, 26(2):319–324, 1955.
- K. Maboudi, E. Ackermann, L. W. de Jong, B. E. Pfeiffer, D. Foster, K. Diba, and C. Kemere. Uncovering temporal structure in hippocampal output patterns. *Elife*, 7, June 2018.
- S. N. MacEachern. Estimating normal means with a conjugate style Dirichlet process prior. *Communications in Statistics - Simulation and Computation*, 23(3):727–741, Jan. 1994.
- E. L. Mackevicius, A. H. Bahle, A. H. Williams, S. Gu, N. I. Denisenko, M. S. Goldman, and M. S. Fee. Unsupervised discovery of temporal sequences in high-dimensional datasets, with applications to neuroscience. *Elife*, 8, Feb. 2019.
- H. Mei and J. Eisner. The neural Hawkes process: A neurally self-modulating multivariate point process. *arXiv preprint arXiv:1612.09328*, 2016.

- J. W. Miller and M. T. Harrison. Mixture models with a prior on the number of components. *J. Am. Stat. Assoc.*, 113(521):340–356, 2018.
- G. Mohler, J. Carter, and R. Raje. Improving social harm indices with a modulated Hawkes process. *International Journal of Forecasting*, 34(3):431–439, 2018.
- G. O. Mohler, M. B. Short, P. J. Brantingham, F. P. Schoenberg, and G. E. Tita. Self-exciting point process modeling of crime. *Journal of the American Statistical Association*, 106(493):100–108, 2011.
- J. Møller and H. Toftaker. Geometric anisotropic spatial point pattern analysis and Cox processes: Anisotropic point pattern analysis. *Scand J Statist*, 41(2):414–435, June 2014.
- J. Møller and R. P. Waagepetersen. *Statistical Inference and Simulation for Spatial Point Processes*. Taylor & Francis, Sept. 2003.
- J. Møller, A. R. Syversveen, and R. P. Waagepetersen. Log Gaussian Cox processes. *Scandinavian Journal of Statistics*, 25(3):451–482, 1998.
- P. Müller and A. Rodriguez. Dependent Dirichlet processes and other extensions. In *Nonparametric Bayesian Inference*, pages 53–75. Institute of Mathematical Statistics, 2013.
- R. M. Neal. Bayesian mixture modeling. In *Maximum Entropy and Bayesian Methods*, pages 197–211. Springer, 1992.
- R. M. Neal. Markov chain sampling methods for Dirichlet process mixture models. *J. Comput. Graph. Stat.*, 9(2):249–265, June 2000.
- J. Neyman and E. L. Scott. Statistical approach to problems of cosmology. *J. R. Stat. Soc. Series B Stat. Methodol.*, 20(1):1–29, Jan. 1958.
- A. Nobile. *Bayesian Analysis of Finite Mixture Distributions*. PhD thesis, Carnegie Mellon University, 1994.
- P. Orbanz. Lecture Notes on Bayesian Nonparametrics. [http://www.gatsby.ucl.ac.uk/~porbanz/papers/porbanz\\_BNP\\_draft.pdf](http://www.gatsby.ucl.ac.uk/~porbanz/papers/porbanz_BNP_draft.pdf), 2014. [Online; accessed 30-July-2021].
- S. Peter, E. Kirschbaum, M. Both, L. Campbell, B. Harvey, C. Heins, D. Durstewitz, F. Diego, and F. A. Hamprecht. Sparse convolutional coding for neuronal assembly detection. In I. Guyon, U. V. Luxburg, S. Bengio, H. Wallach, R. Fergus, S. Vishwanathan, and R. Garnett, editors, *Advances in Neural Information Processing Systems 30*, pages 3675–3685. Curran Associates, Inc., 2017.
- D. B. Phillips and A. F. Smith. Bayesian model comparison via jump diffusions. *Markov chain Monte Carlo in practice*, 215:239, 1996.
- J. Pitman. *Combinatorial Stochastic Processes: Ecole d’Été de Probabilités de Saint-Flour XXXII – 2002*. Springer, Berlin, Heidelberg, 2006.
- J. Pitman and M. Yor. The two-parameter Poisson-Dirichlet distribution derived from a stable subordinator. *Annals of Probability*, 25(2):855–900, Apr. 1997.
- P. Quaglio, V. Rostami, E. Torre, and S. Grün. Methods for identification of spike patterns in massively parallel spike trains. *Biol. Cybern.*, 112(1-2):57–80, Apr. 2018.

- J. G. Rasmussen. Bayesian inference for Hawkes processes. *Methodology and Computing in Applied Probability*, 15(3):623–642, 2013.
- S. Richardson and P. J. Green. On Bayesian analysis of mixtures with an unknown number of components (with discussion). *J. R. Stat. Soc. Series B Stat. Methodol.*, 59(4):731–792, 1997.
- B. D. Ripley. Modelling spatial patterns. *J. R. Stat. Soc. Series B Stat. Methodol.*, 39(2):172–212, 1977.
- E. Russo and D. Durstewitz. Cell assemblies at multiple time scales with arbitrary lag constellations. *Elife*, 6, Jan. 2017.
- A. Schein, S. Linderman, M. Zhou, D. Blei, and H. Wallach. Poisson-randomized gamma dynamical systems. *Advances in Neural Information Processing Systems*, 32:782–793, 2019.
- C. R. Shelton, Z. Qin, and C. Shetty. Hawkes process inference with missing data. In *Thirty-Second AAAI Conference on Artificial Intelligence*, 2018.
- A. Simma and M. I. Jordan. Modeling events with cascades of Poisson processes. *Proceedings of the Conference on Uncertainty in Artificial Intelligence*, 2010.
- P. Smaragdis. Convolutional speech bases and their application to supervised speech separation. *IEEE Trans. Audio Speech Lang. Processing*, 2006.
- T. Smith. Hostages freed as Israelis raid Uganda airport. *The New York Times*, Jul 1976.
- D. Stoyan and A. Penttinen. Recent applications of point process methods in forestry statistics. *Statistical science*, pages 61–78, 2000.
- D. Stoyan and H. Stoyan. Estimating pair correlation functions of planar cluster processes. *Biom. J.*, 38(3):259–271, 1996.
- U. Tanaka and Y. Ogata. Identification and estimation of superposed Neyman–Scott spatial cluster processes. *Ann. Inst. Stat. Math.*, 66(4):687–702, Aug. 2014.
- U. Tanaka, Y. Ogata, and D. Stoyan. Parameter estimation and model selection for Neyman-Scott point processes. *Biometrical Journal: Journal of Mathematical Methods in Biosciences*, 50(1):43–57, 2008.
- M. Thomas. A generalization of Poisson’s binomial limit for use in ecology. *Biometrika*, 36(Pt. 1-2): 18–25, June 1949.
- A. Verma, S. G. Jena, D. R. Isakov, K. Aoki, J. E. Toettcher, and B. E. Engelhardt. A self-exciting point process to study multicellular spatial signaling patterns. *Proceedings of the National Academy of Sciences*, 118(32), 2021.
- R. P. Waagepetersen. An estimating function approach to inference for inhomogeneous Neyman-Scott processes. *Biometrics*, 63(1):252–258, 2007.
- T. Wang, M. Bebbington, and D. Harte. Markov-modulated Hawkes process with stepwise decay. *Annals of the Institute of Statistical Mathematics*, 64(3):521–544, 2012.
- S. Wheatley, V. Filimonov, and D. Sornette. The Hawkes process with renewal immigration & its estimation with an EM algorithm. *Computational Statistics & Data Analysis*, 94:120–135, 2016.

- T. Wiegand and K. A. Moloney. *Handbook of Spatial Point-Pattern Analysis in Ecology*. CRC Press, Dec. 2013.
- A. Williams, A. Degleris, Y. Wang, and S. Linderman. Point process models for sequence detection in high-dimensional neural spike trains. In H. Larochelle, M. Ranzato, R. Hadsell, M. F. Balcan, and H. Lin, editors, *Advances in Neural Information Processing Systems*, volume 33, pages 14350–14361. Curran Associates, Inc., 2020a.
- A. H. Williams, B. Poole, N. Maheswaranathan, A. K. Dhawale, T. Fisher, C. D. Wilson, D. H. Brann, E. M. Trautmann, S. Ryu, R. Shusterman, D. Rinberg, B. P. Ölveczky, K. V. Shenoy, and S. Ganguli. Discovering precise temporal patterns in large-scale neural recordings through robust and interpretable time warping. *Neuron*, 105(2):246–259.e8, Jan. 2020b.
- S. Wold. Cross-validatory estimation of the number of components in factor and principal components models. *Technometrics*, 20(4):397–405, 1978.
- R. L. Wolpert and K. Ickstadt. Poisson/gamma random field models for spatial statistics. *Biometrika*, 85(2):251–267, June 1998.
- J. Wu, O. Ward, J. Curley, and T. Zheng. Markov-modulated Hawkes processes for sporadic and bursty event occurrences. *arXiv preprint arXiv:1903.03223*, 2019.
- Q. Zhang, A. Lipani, O. Kirnap, and E. Yilmaz. Self-attentive Hawkes process. In *International Conference on Machine Learning*, pages 11183–11193. PMLR, 2020a.
- R. Zhang, C. Walder, and M.-A. Rizoïu. Variational inference for sparse Gaussian process modulated Hawkes process. *Proceedings of the AAAI Conference on Artificial Intelligence*, 34(04):6803–6810, Apr. 2020b. doi: 10.1609/aaai.v34i04.6160.
- K. Zhou, H. Zha, and L. Song. Learning social infectivity in sparse low-rank networks using multi-dimensional Hawkes processes. *Proceedings of the International Conference on Artificial Intelligence and Statistics*, 16, 2013.
- S. Zuo, H. Jiang, Z. Li, T. Zhao, and H. Zha. Transformer Hawkes process. In *International Conference on Machine Learning*, pages 11692–11702. PMLR, 2020.